Spring 2008

Roles of gap junctions in neuronal networks

Joon Ha
New Jersey Institute of Technology

ABSTRACT

ROLES OF GAP JUNCTIONS IN NEURONAL NETWORKS

by
Joon Ha

This dissertation studies the roles of gap junctions in the dynamics of neuronal networks in three distinct problems. First, we study the circumstances under which a network of excitable cells coupled by gap junctions exhibits sustained activity. We investigate how network connectivity and refractory length affect the sustainment of activity in an abstract network. Second, we build a mathematical model for gap junctionally coupled cables to understand the voltage response along the cables as a function of cable diameter. For the coupled cables, as cable diameter increases, the electrotonic distance decreases, which cause the voltage to attenuate less, but the input of the second cable decreases, which allows the voltage of the second cable to attenuate more. Thus we show that there exists an optimal diameter for which the voltage amplitude in the second cable is maximized. Third, we investigate the dynamics of two gap-junctionally coupled theta neurons. A single theta neuron model is a canonical form of Type I neural oscillator that yields a very low frequency oscillation. The coupled system also yields a very low frequency oscillation in the sense that the ratio of two cells' spiking frequencies obtains the values from a very small number. Thus the network exhibits several types of solutions including stable suppressed and $1 : N$ spiking solutions. Using phase plane analysis and Denjoy's Theorem, we show the existence of these solutions and investigate some of their properties.

ROLES OF GAP JUNCTIONS IN NEURONAL NETWORKS

by

Joon Ha

A Dissertation
Submitted to the Faculty of
New Jersey Institute of Technology and
Rutgers, The State University of New Jersey – Newark
in Partial Fulfillment of the Requirements for the Degree of
Doctor of Philosophy in Mathematical Sciences

Department of Mathematical Sciences
Department of Mathematics and Computer Science, Rutgers-Newark

May 2008

APPROVAL PAGE

ROLES OF GAP JUNCTIONS IN NEURONAL NETWORKS

Joon Ha

4-29-08

Amitabha Bose, Dissertation Advisor   Date
Professor, Department of Mathematical Sciences, NJIT

4/29/08

Farzan Nadim, Committee Member   Date
Professor, Department of Mathematical Sciences, NJIT and Department of
Biological Sciences, Rutgers-Newark

4/29/08

Jorge Golowasch, Committee Member   Date
Associate Professor, Department of Mathematical Sciences, NJIT and Department
of Biological Sciences, Rutgers-Newark

04/29/08

Horacio Rotstein, Committee Member   Date
Assistant Professor, Department of Mathematical Sciences, NJIT

04.29.08

Georgi Medvedev, Committee Member   Date
Assistant Professor, Department of Mathematics, Drexel University

BIOGRAPHICAL SKETCH

Author: Joon Ha

Degree: Doctor of Philosophy

Date: May 2008

Undergraduate and Graduate Education:

- Doctor of Philosophy in Mathematical Sciences,
  New Jersey Institute of Technology, Newark, NJ, 2008

- Master of Science in Applied Mathematics,
  Brown University, Providence, RI, 2002

- Master of Science in Mathematics,
  Hanyang University, Seoul, Korea, 1996

- Bachelor of Science in Mathematics,
  Hanyang University, Seoul, Korea, 1991

Major: Mathematical Sciences

Presentations and Publications:

J. Ha, A. Bose, F. Nadim, and J. Golowasch. "Sustainment of activity in neuronal networks coupled by gap junctions," *Contributed talk, SIAM Conference on Applications of Dynamical Systems*, Snowbird, UT, May 2007.

In memory of my grandmother, Bongim Seok.

For my wife, Junghwa and my kids, Jiwoo and Jean.

ACKNOWLEDGMENT

First of all, I would like to express my gratitude to my advisor, Dr. Amitabha Bose who has been abundantly helpful and offered invaluable assistance, support and guidance. I would like to thank Dr. Farzan Nadim and Dr. Jorge Golowasch for helping and guiding me to perform research on cable theory and taking the time to discuss their previous works with me several times. I would also like to thank my committee members Dr. Horacio Rotstein and Dr. Georgi Medvedev who read my thesis and guided me. I would like to thank many faculty members in the Department of Mathematical Sciences at NJIT. In particular, I would like to thank Dr. Victor Matveev and Dr. Gregory Kriegsmann for taking the time to discuss several topics related to my thesis and the electrical circuit theory.

I would like to thank Myoungkeun Oh, for helping me out in learning LaTex, Powerpoint and helping me improve my computational skills. I would also like to thank Lakshmi Chandrasekaran, for sharing and discussing many things as a graduate student with me. I would like to thank my cousin, Changwoo Chung and my friends Dongkeun Lee and Sanggyun Han and for installing Linux and other software in my laptop and supporting me in many ways. I would also like to thank pastor Jungin Han for his prayer.

Finally, this research would not have been possible without the support of my wife, Junghwa Lee. I am deeply indebted to Junghwa. I would like to express my thanks to my parents, Jongsang Ha and Jungja Chung and my brothers and sister, Youngjun Ha, Sejun Ha, Heejun Ha and Kyounghwa Ha, for their support throughout this process. I would also like to thank my brother-in-law and sister-in-law, Jungwoon Park and Misook Lee, for their prayers and financial support. My special thanks go to my mother-in-law and brother-in-law, Hyosun Kim and Kangnam Lee for their prayers. I would like to express my gratitude to my uncle Bal Chung and aunt Munja

TABLE OF CONTENTS

TABLE OF CONTENTS
(Continued)

LIST OF FIGURES

Figure   **Page**

CHAPTER 1

INTRODUCTION

Individual nerve cells, called neurons, receive inputs from numerous other neurons. By integrating inputs neurons create new information and sends it out to other cells. Neurons use electrical signals to process information through changes in voltage across their cell membranes. The membrane contains ion channels that selectively allows ions, such as Na^+, K^+, Ca^{2+}, Cl^-, to move across the cell membrane. When current flows across the cell membrane, it may change the membrane potential to a more positive value or negative value called depolarization and hyperpolarization, respectively.

If a neuron is depolarized sufficiently so that the membrane potential goes above a threshold, the neuron generates an action potential, characterized by a fast increase and subsequent decrease in membrane potential. The only forms of membrane potential changes that can spread rapidly over long distances are action potentials. Neurons transmit their information by firing sequences of action potentials in various temporal patterns.

Two important morphological features of neurons are the dendrites that receive inputs from other neurons and the axon that transmits the neuronal information to other cells. The branching structure of the dendritic trees allows a neuron to receive inputs from many other neurons through connections called synapses.

Synapses are classified into two major groups: electrical synapses and chemical synapses. In this thesis, we focus on the former. At electrical synapses, current flows directly into the post synaptic cell through specialized bridging channels, gap-junction channels. These channels have low resistance and high conductance. A gap junction is formed by a pair of connexons, proteins that form aqueous channels between the

1

cytoplasms of adjacent cells, each cell contributing one connexons. Transmission across electrical synapses is very fast. There is much evidence showing the presence of gap junctions in neuronal networks [1]. The role of gap junctions for a two compartment model neuron has been studied by several authors [2, 3, 4]. Lewis and Rinzel studied the influence of the strength of gap junctions to promote anti-synchrony or synchrony in spiking neuron models where the suprathreshold effect of a spike is artificially modeled [2]. Ermentrout showed that gap junctions between excitable neurons disrupts the persistent state of network activity [3]. Chow and Kopell showed the existence and stability of phase-locked neurons coupled electrically with gap junctions. They showed that the role of gap junctions can be considered as combining the effects of excitation and inhibition of synapses [4]. To see this, in the spiking phase of one cell, the coupling current to the other cell is depolarizing, acting like excitation; in the postpolarization phase, these currents can be hyperpolarizing like inhibition. So gap junctions have both excitatory and inhibitory effects. They also showed that the stability of synchronous solution mainly comes from the effects of spikes. Lewis described the existence and stability of phase-locked solutions as a function of the coupling strength and a spike effect parameter for two electrically coupled non-leaky Integrate-And-Fire model neurons [5]. This model allows both synchrony and anti-synchrony to be stable in some parameter regions.

Weakly connected networks can be reduced to a phase model which is more amenable to analysis [6]. All-to-all coupled networks [7], chains of oscillators with the nearest-neighbor coupling [8, 9, 10], and chains of oscillators beyond the nearest-neighbor [11] have been studied to illustrate phase-locked solutions. Specifically, for any system of weakly coupled, nearly identical oscillators, Kuramoto used a mean field approximation to decouple the system [12].

For non-weakly connected networks, Medvedev and Kopell investigated synchronization in chains of electrically coupled Fitzhugh-Nagumo oscillators [13].

Their model was motivated by dopamine-releasing neurons [14]. A single such cell was modeled by a chain of oscillators (compartments) with different gating dynamics. Between compartments, very strong electrical coupling strength was assumed. This model showed synchronous oscillations and yielded transient dynamics. Chow and Kopell [4] also showed that all-to-all coupled network can exhibit a splay-phase state by using the spiking response method [15].

Yet up to 98% of neuronal surface area is composed of dendritic trees. Most cells possess highly branched and extensive dendritic trees. A cable theory in the nervous system has been developed by several authors to understand these extensive systems [16, 17, 18]. This cable theory can be applied to spatially dependent neurons, axon or sections of dendrites which closely resemble a cylinder. Rall built a core conductor model to understand the current flow in nervous cells [17]. The membrane resistivity of dendrite is very high compared to the intracellular cytoplasm. Thus, the radial and angular components of the current flow can be neglected. The $3 - D$ cable problem can be reduced to a $1 - D$ problem.

The overall goal of this thesis is to investigate the role of gap junctions in neuronal networks. We consider three distinct problems all related to the role of gap junctions in neuronal networks. Two of them are motivated directly by the work of Nadim and Golowasch [19], while the third is primarily of mathematical interest. We first describe the first two components.

Gansert, Nadim and Golowasch studied sustained periodic activity in a randomly connected electrical coupled neuronal network as a function of cable diameter [19]. They extracted a sub-network that contains at least one ring-like structure by using a detection algorithm, which they refer to as the kernel of network activity. The role of the kernel of network activity is to localize the sustained activity to be within this sub-network. They also found the existence of an optimal dendrite diameter such that

action potentials propagate through the network for diameters in a neighborhood of the optimal.

We are also interested in understanding sustained activity of gap junctionally coupled cables network. Here sustained activity means periodic activity. We first consider non-biophysical gap junctionally coupled neurons to develop rules on network architecture that will allow sustained activity to occur. We assume several rules on activity propagation to simplify the structure of the network and show some simple network architectures that sustain activity. We determine rules on network architecture that allow activity to be sustained in the context of Graph Theory. Specifically, we investigate how the sustainment of activity depends on network connectivity, the refractory period of each neuron and the number of associated paths. A necessary condition for sustainment of activity is the existence of a closed path. A node is said to be a cut-off node if its removal from the network leaves it to be a sub-network that does not contain any closed paths. Thus, whether activity is sustained can be deduced by knowing whether activity propagates through a cut-off node. Specifically, given a cut-off node i with n connections, we would like to know how many in-flowing $I(i, t^-)$ and out-flowing $O(i, t^+)$ currents at a discrete time t are required for activity to propagate through the cut-off node at time t. We have found that whether an action potential propagates through a cut-off node with n connections at a discrete time t ends up with knowing whether the ratio of in-flowing currents to out-flowing currents associated with these paths is greater than the threshold.

Recently, Nadim and Golowasch have studied how the effectiveness of signal transmission between two gap junctionally coupled passive linear cables depends on cable diameter [20]. They determined the voltage response of the second cable in response to a step voltage clamp at the beginning of the first cable. They measured the steady state response as a function of the strength of coupling resistance, diameter of the cable and cell membrane properties. They have showed numerically that there

exists an optimal diameter of the cable where the signal can be transmitted most effectively along the coupled cables.

In the second part of the thesis, we determine the voltage response of two gap junctionally coupled passive cables as a function of cable diameter d. Specifically, when the proximal end of the first cable is voltage-clamped, we investigate the voltage response along the second cable and establish a general condition for the existence of an optimal diameter. In a single cable model, the cable diameter is explicitly included in the diffusion coefficient which is proportional to $\sqrt{d}$. Thus, as d increases, the voltage response increases. However, the voltage response of the second cable for two gap junctionally coupled cables does not simply increase.

The third part of the thesis considers the theta neuron model which is a canonical form of a Type 1 membrane oscillator that yields a very low frequency oscillation via a saddle node bifurcation [21]. We have studied the dynamics of two such neurons coupled by gap junctions. Depending on an intrinsic parameter I of the theta neuron and on the coupling strength g_c, the network exhibits several types of solutions including stable suppressed, $1 : N$ and $1 : 1$ spiking solutions. Here a suppressed solution and $1 : N$ spiking solution are the solutions that have the ratio of two cells' spiking frequencies as 0 and $\frac{1}{N}$, respectively. We use a geometric approach of dynamical systems to construct many of the above mentioned solutions.

CHAPTER 2

SUSTAINED ACTIVITY IN AN ABSTRACT NEURONAL NETWORK

We consider a network of identical point neurons coupled by gap junctions where each uncoupled cell is a near oscillator. An action potential in one cell causes current to pass between two coupled point cells. When a stimulus is applied to a network, we would like to know whether activity propagates through the network. In this section, we determine rules on network architecture that allow activity to continue to be propagated. In this chapter, we will:

1. Establish general rules on network architecture that allow activity to be sustained.

2. Provide several example networks that exhibit sustained activity.

3. Identify nodes that are critical for sustained activity (called sup cut-off nodes) and derive relationships between the refractory state, input/output load on a neuron and the length of paths associated with sup cut-off nodes needed to sustain activity.

2.1 Assumptions to Build an Abstract Network

We consider an abstract structure without any biological realism. We consider each cell to be a node within a directed graph. There are several assumptions that we shall make to simplify the structure of the graph. We will assign rules for how activity moves through the graph and will thereby consider the network as a discrete dynamical system.

Assumption 2.1.1 Each cell is identical.

Assumption 2.1.2 When a cell fires, we define the propagation time until the activity reaches a coupled cell as one unit of time. The propagation time between any two cells in the network is the same.

6

Assumption 2.1.3 When a cell fires, the current can flow to any directly connected cells, which may cause them to fire at the next time step.

Assumption 2.1.4 One cell can be connected to several nearby cells by gap junctions through multiple branches.

Each branch might not pass enough current to allow the coupled cell to fire. However, if several in-flowing currents merge in a cell simultaneously, then the total current at that moment may be large enough to trigger a cell to fire.

Definition 2.1.5 The number of out-flowing currents of node i (cell i) at time step t is denoted by $O(i, t^+)$ and the number of in-flowing currents of node i (cell i) at time step t by $I(i, t^-)$.

Definition 2.1.6 The degree of node i denoted by $d(i)$ is the number of cells directly connected to it. Note that $d(i)=O(i, t^+) + I(i, t^-)$ where activities pass through node i at time step t.

Definition 2.1.7 The current flux of node i at time step t is denoted by $u(i, t)$ as $\frac{I(i,t^-)}{O(i,t^+)}$.

Assumption 2.1.8 When the current flux $u(i, t)$ is above a prescribed threshold, activity is able to propagate through the node i at the given time step t. We assume that the threshold is $\frac{1}{2}$ throughout this section.

Assumption 2.1.9 Each cell has a refractory period. In other words, once a cell fires, there is a subsequent period of time that it cannot fire, independent of the current flux $u(i, t)$. We assume that the refractory period is two throughout this section.

Note that each cell has its own initial refractory state $(0, 1, 2)$. A cell having 0 refractory state is ready to fire if a large enough current flows in. On the other hand, a cell having 1 (2) refractory state needs to wait for one (two) more time steps in order to be ready to fire. We assume that there is no way for a refractory state 1 or 2 cell to fire even when a large enough current comes in.

2.2   When Does Activity in the Network Die Off?

We consider a network which is subject to the assumptions in section 2.1. To see the roles of the assumptions, we look at some simple network structures through which activity fails to propagate.

Example 2.2.1 Assume that the initial refractory state of each cell is equal to 0 and every cell is connected to all other cells. If a stimulus causes one cell to fire, then all other cells fire at the next time step (assume the initial current flux at the stimulated cell is above threshold). Due to the refractory period, no cells are able to fire at the next time step and the network activity dies. This example implies that in order for activity to propagate, a network in which all cells have the same initial refractory state should not have the maximum number of connections at each node.

Example 2.2.2 Assume that the initial refractory state for each cell is equal to 0 and the network has a circular structure. Thus each node is connected to only two nearby cells. Then each cell has degree 2 and there are no ways that activity can propagate through the network. A stimulated cell invokes two nearby cells to fire and the activity propagates in both directions (clock-wise and counter clock-wise). Eventually the two activities meet or are next to each other (depending on the number of cells in a network). At this point, activity cannot propagate through this node due to the refractory period. Example 2.2.2 shows that the degree of every node should not be too small. However, if a cell is stimulated and another cell within a distance 1 (2) of the stimulated cell has an initial refractory state 1 (2), then activity arriving from the stimulated cell to this cell will die off. But activity also propagates from the stimulated node in the opposite direction and thus can be sustained (the minimum number of cells required in the network is 5, based on the choice of parameters).

Note that nodes having different initial refractory states within a neighborhood of the stimulated cell influence network activity. We first analyze network activity
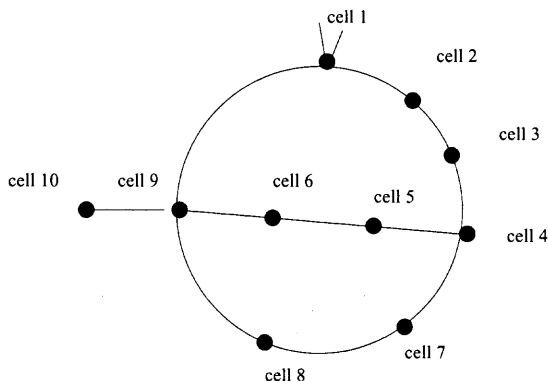
Figure 2.1 Cell 1 is stimulated, activity propagates through cell 9 and thus activity is sustained.

in the case of the same initial refractory state 0 in a network and then study how a node having different initial refractory state changes network activity.

Example 2.2.3 Assume that the initial refractory state for each cell is equal to 0 and the network has a structure as shown in Figure 2.1. If cell 1 is stimulated, activity propagates in both directions (counter clock-wise and clock-wise). The counter clock-wise activity dies off at cell 9 because $u(9,1)$ is $\frac{1}{3}$. On the other hand, the clock-wise activity propagates through cell 2 and cell 3 and then branches after cell 4. When the activity arrives at cell 9 via the upper branch (cell 5, 6, 9), the current is not enough to trigger cell 9. However, a second wave of activity comes into cell 9 via the lower branch (cell 7, 8, 9) at the same moment. Thus the in-flowing current to cell 9 is enough to trigger it since $u(9,6)=1$. Activity propagates to cell 10 but it dies off there because it is unable to back propagate to cell 9 to fire due to its refractory period. Thus, activity propagates to only cell 1 and the cycle repeats. Therefore, this network sustains its activity.

Example 2.2.3 shows that even at a node with large degree, if another current comes into it at the appropriate time, the activity can propagate through the cell. The appropriate time is related to the length of branches. For example, if the upper

branch includes only cell 5 and now the length of upper branch is 2, then the upper activity dies at cell 9 and the lower branch activity also dies there.

From these examples, we conclude that the main parameters that affect whether a network stays alive are the degree of a node, the refractory period, and the lengths of paths (branches). Since we assumed that the refractory period is fixed in the network, neuronal network structure really results from the degree of each node and length of each path.

2.3   Activity Patterns and Mathematical Descriptions

In the context of graph theory, a graph consists of a set of objects called nodes and another set called edges. Here we regard each cell as a node and a connection as an edge. We build a neuronal network based on graph theory and state some definitions associated with it found in [22].

Definition 2.3.1 A walk is defined as a finite alternating sequence of nodes and edges, beginning and ending with nodes. Terminal nodes refer to nodes with which a walk begins and ends.

Definition 2.3.2 A walk is said to be path if no node appears more than once.

Definition 2.3.3 A path is said to be a closed path if its terminal nodes are the same.

Definition 2.3.4 A network is said to be connected if there is at least one path between every pair of nodes in a network.

Now we consider networks that can exhibit several types of activities. Throughout this section, we assume that each cell has initial refractory state 0. We also assume that there exists one node in a network which is a member of at least two closed paths. If there is no such node in a network, the activity cannot be sustained as in example 2.2.2. Note that in the network shown in Figure 2.1, cell 9 is a member of two closed paths (1-2-3-4-7-8-9 and 1-2-3-4-5-6-9).
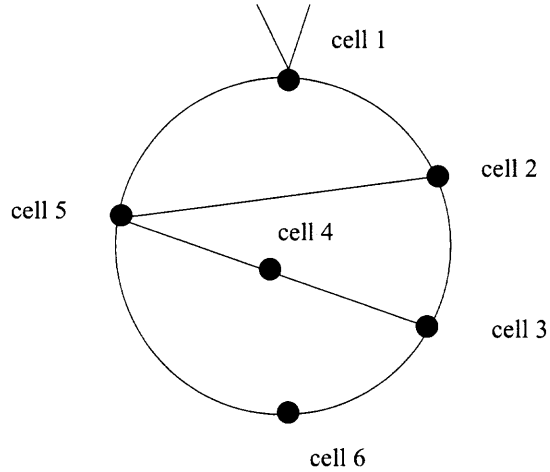
Figure 2.2 Cell 1 is stimulated, activity comes back to cell 1 but is unable to propagate through it. However, activity is sustained within a sub-network(cell 2, 3, 4, 5 and 6).

When a node is stimulated, it may yield several types of activity patterns which depend on its structure and the location within the network of the stimulated node.

Type 1 Periodic activity: Activity propagates back to the initial stimulated cell, continues to propagate through the initial stimulated node and thus the activity is sustained (see Figure 2.1).

Type 2 Triggering activity: There is no periodic activity through a stimulated node but it triggers periodic sustained activity within a sub-network (see Figure 2.2).

Note that it is possible that activity fails to propagate through the initial stimulated node even if activity propagates back to it (see Figure 2.2). To see this, when cell 1 is stimulated, the counter clock-wise activity dies off at cell 5 since $u(5,1) = \frac{1}{3}$. The clock-wise activity propagates only to cell 3 through cell 2 since $u(5,2) = \frac{1}{3}$. At t=4, the two activities merge in cell 5. Now $u(5,4)$ is 1, which is enough to trigger cell 5. One path of activity propagates back to cell 1 but is unable to propagate through cell 1 and dies off there. On the other hand, the other path of activity (cell 5 to cell 2) becomes a cycle (5-2-3-(4,6)-5).
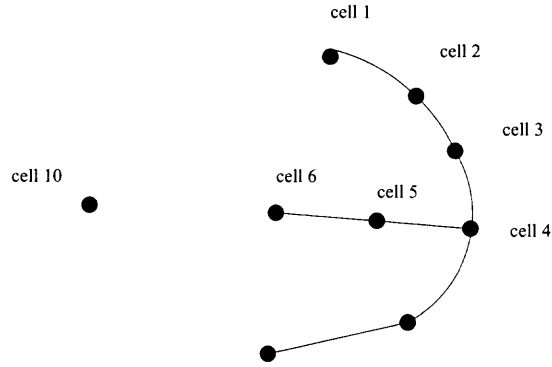
Figure 2.3 Cell 9 of Figure 2.1 is a sup cut-off node: Over-loaded cell 9's removal from Figure 2.1 network yields a sub-network that does not contain any closed path.

2.4 Classification of Nodes According to Their Structure and Activity Propagation through a Sup cut-off Node

In this section, nodes are classified according to their network structure.

Definition 2.4.1 A node i is said to be a cut-off node if its removal from the network leaves a sub-network that does not contain any closed paths (see Figure 2.3 and 2.4).

A cut off node is very crucial to sustained activity because any activity must propagate through it.

Definition 2.4.2 A node i is said to be an over-loaded node if $3 < d(i)$.

Note that $3 < d(i)$ is equivalent to $\frac{1}{d(i)-1} < \frac{1}{2}$. In other words, if one in-flowing current is not enough to trigger a node, then it is said to be an over-loaded node.

In order for activity to propagate through an over-loaded node, more than one current should simultaneously flow in to this node.

Definition 2.4.3 A node is said to be a sup cut-off node if it is a cut-off and over-loaded node (see Figure 2.3). A node is said to be a sub cut-off node if it is a cut-off and non over-loaded node (see Figure 2.4).

Whether activity is sustained can be deduced by knowing whether activity propagates through a sup cut-off node. Specifically, given a sup cut-off node, we
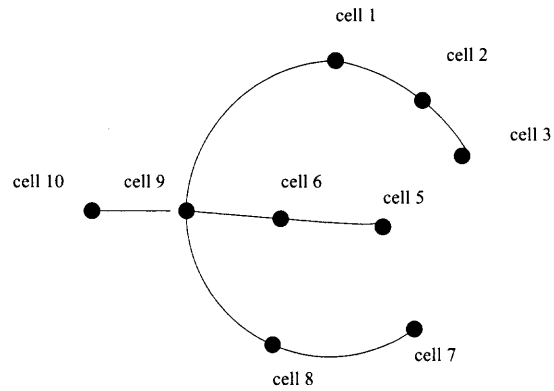
Figure 2.4 Cell 4 of Figure 2.1 is a sub cut-off node: non over-loaded cell 4's removal from Figure 2.1 network leaves a sub-network that does not contain any closed paths.
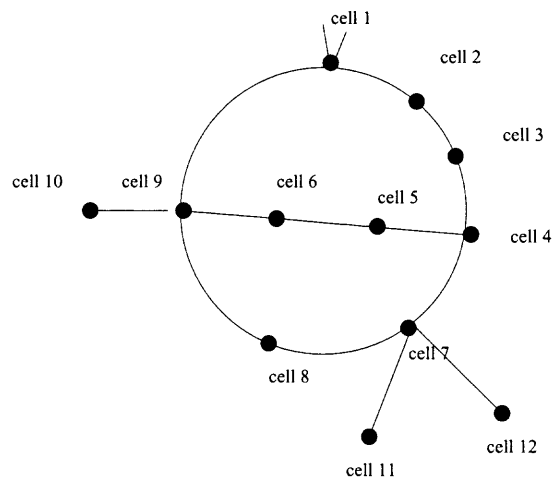
Figure 2.5 Cell 7 is not a cut-off but an over-loaded node. Cell 7's removal from the network leaves a sub-network that still contains a closed path.

would like to know how many in-flowing currents are required for activity to propagate through it. Denote the smallest integer greater than a real number x by $< x >$.

Lemma 2.4.4 $< \frac{d(i)}{3} > \leq I(i, t^-) < d(i)$ if and only if activity propagates through a sup cut-off node i at time step t.

Proof of Lemma 2.4.4

The condition for activity to pass through a sup cut-off node i at time step t is that $\frac{I(i,t^-)}{d(i)-I(i,t^-)} \geq \frac{1}{2}$. Then $I(i, t^-) \geq \frac{d(i)}{3}$, $I(i, t^-)$ is an integer and smaller than $d(i)$. Thus, $< \frac{d(i)}{3} > \leq I(i, t^-) < d(i)$.

Now we study a simple network that has only one sup cut-off node (possibly some sub cut-off nodes but no other over-loaded nodes). First, we determine under what conditions on network structure activity propagates from a stimulated node to a sup cut-off node.

Definition 2.4.5 A path is said to be associated with a stimulated node a if the path begins with node a.

Definition 2.4.6 An edge of node i is said to be associated with a stimulated node a if there exists a path associated with stimulated node a that ends with node i.

Let $d_a(i)$ denote the number of edges of node i associated with a stimulated node a (see Figure 2.5). For example, the edge between cell 9 and cell 10 is not an edge of node 9 associated with stimulated node 1.

Lemma 2.4.7 Assume that node i is the only sup cut-off node in a network, then $d_a(i)$ is exactly the number of paths associated with a stimulated node a and ending with node i.

Proof of Lemma 2.4.7

Denote the number of paths associated with a stimulated node a and ending with i by $P(a, i)$. Obviously, $d_a(i) \leq P(a, i)$ because the network is connected. Suppose that $d_a(i) < P(a, i)$. Then, some of the edges of i are shared by 2 distinct paths.

Thus, there exists a second closed sub-network that does not contain node i, which contradicts the fact that node i is the only sup cut-off node.

Lemma 2.4.7 implies that any two paths beginning with node a and ending with node i can only merge at node i.

Theorem 2.4.8 Assume that a node i is the only sup cut-off and over-loaded node in the network and the initial refractory state for each cell is equal to 0, then $I(i, k^-)$ is exactly the number of all paths with length k which are associated with node a and end with node i.

Proof of Theorem 2.4.8

Denote the number of all paths with length k which are associated with node a and end with node i by $P(a, i, k)$. Obviously, $I(i, k^-) \leq P(a, i, k)$. Suppose that $I(i, k^-) < P(a, i, k)$, then either 1) two waves of activity merge in a node at a time step $t < k$ or 2) one of them dies off due to the refractory period or at an over-loaded node. If the two waves of activity merge in node j, then there exists a closed path including node j that does not contain node i, which contradicts again the fact that node i is the only sup cut-off node. So 1) can be excluded. In order for activity to die off due to the refractory period without being merged, the two waves of activity must come next to each other at a given time step on a path. As in 1), they also have a node in common. Therefore, there must be a closed path in a network, which contradicts again the fact that node i is the only sup cut-off node. Hence, 2) can be excluded.

From Lemma 2.4.4 and Theorem 2.4.8, if a node a is stimulated, then a necessary and sufficient condition that activity propagates through a sup cut-off node i at a time step k is $< \frac{d(i)}{3} > \leq P(a, i, k) < d(i)$. The number of all paths with length k which start with a and end with i must exceed the smallest integer greater than a third of the degree of the sup cut-off node i at time step k in order to propagate through the node i.

cell 1

cell 5

cell 6

cell 3

cell 2

cell 4 (intitial refractory state 2)
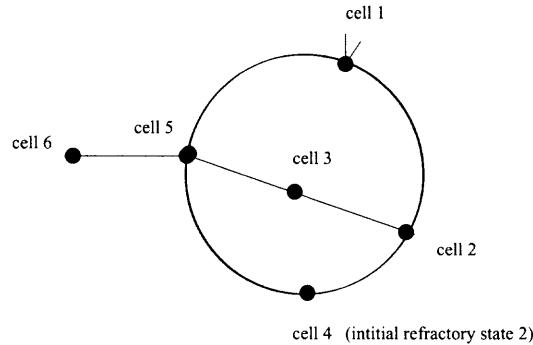
Figure 2.6 Cell 5 is a cut-off and cell 4 has the initial refractory state 2 and $P(1, 5, 3) = 2, R(1, 5, 4, 3) = 1, I(5, 3^-) = 1$. Thus activity cannot propagate through cell 5 at time step 3.

Now we consider the situation where all cells do not necessarily begin in the same refractory state.

Corollary 2.4.9 If a node b in a neighborhood of a stimulated node a has a different initial refractory state and $R(a, i, b, k)$ denotes the number of all paths with length k associated with node a that contain a node b and end with node i, then $I(i, k^-)$ is $P(a, i, k) - R(a, i, b, k)$.

Example 2.4.10 As shown in Figure 2.6, cell 5 is a sup cut-off node and cell 4 has the initial refractory state 2. The initial states of all other cells are 0. Cell 1 is stimulated and activity dies at cell 5 since $u(5, 1) = \frac{1}{3}$, but propagates through cell 2 since $u(2, 1) = \frac{1}{2}$. However, at this time step, the refractory state of cell 4 is one. Thus the activity through cell 2 can only propagate to cell 3. Thus $u(5, 3) = \frac{1}{3}$ and the activity dies. If cell 4 were to start in refractory state 1 or 0, then $u(5, 3) = \frac{1}{2}$ and activity could be sustained.

Lemma 2.4.11 Assume that the same condition as Theorem 2.4.8 holds with $I(i, k^-) = d_a(i) - 1$, if there is only one path l beginning with node a and ending with node i which has no common node with all other paths and has a length less than k, then activity propagates from a sup cut-off node to a stimulated node. The network has a periodic activity.

Proof of Lemma 2.4.11

Since only one path l has a different length (less than k) from all other paths beginning with node a and ending with i, activity along the path dies off at a sup cut-off node before enough current comes in because the current flux is below threshold. However, $I(i, k^-)$ is enough to trigger cell i to fire and activity can propagate into only path l due to the refractory period of the nodes in the other paths. Activity propagates back to a stimulated node a because there are no common nodes with all other paths and thus path l can not invoke any other activity. Once the activity comes back to the stimulated node a, the cycle repeats.

2.5   Conclusion

The results of this chapter show how network architecture influences the possibility of whether a network can exhibit sustained activity. The results also show that understanding architecture alone is not sufficient. One must also take into consideration the refractory state of each node, together with the location of a stimulating node. We provided several examples where changing either of these factors led to a network switching from sustained activity to no activity, or vice versa. We can extend our results to the case of a threshold $\frac{1}{N}$ and a refractory state with $0, 1, 2, \ldots, K$ where M and M are positive integers by simply changing $\frac{I(i,t^-)}{d(i)-I(i,t^-)} \geq \frac{1}{N}$ in Lemma 2.4.4 and $R(a, i, b, k)$ in Corollary 2.4.9. In the case of network architectures having multiple sup cut-off nodes, activity must pass through all sup cut-off nodes. Any paths from one sup cut-off node to another one must not merge in a node other than the two sup cut-off nodes. Thus we can apply Theorem 2.4.8 to this activity propagation. Hence the condition that activity is enable to propagate through two sup cut-off nodes is the same as Theorem 2.4.8. Gap junctionally coupled networks in biological systems are observed in early embryo development stage [23]. The biological system could exhibit sustained activity through gap junctionally coupled networks.

CHAPTER 3

GAP JUNCTIONALLY COUPLED CABLES

A cable theory has been developed to understand the current flow in spatially dependent neurons [17]. We are interested in knowing the voltage response of gap junctionally coupled cables as a function of cable diameter. In the case of a single cable, the voltage attenuation along a single cable increases. The cable electrotonic distance decreases as cable diameter increases. Thus the voltage response increases as cable diameter increases. However, the voltage response of the second cable of gap junctionally coupled cables does not follow the rule. Instead there exists an optimal diameter for which the voltage response can be maximized [20]. Here we build a mathematical model for gap junctionally coupled cables to understand the voltage response of cables in response to arbitrary inputs.

Nadim and Golowasch derived the steady state solution in the form of a system of algebraic equations in response to step voltage clamps. They numerically showed that there exists an optimal diameter for which the maximum voltage response of the second cable occurs. They also gave biophysical reasons for the existence of an optimal diameter.

As mentioned in the previous chapter, Gansert et al. constructed gap junctionally coupled network of model neurons based on the previous Nadim and Golowasch work [19]. They numerically showed that an action potential may propagate through gap junctions for a range of diameters around the optimal value. They also numerically showed that the propagation time can be minimized around this optimal value. They observed that activity can be sustained in the kernel of network activity for a range of optimal diameters.
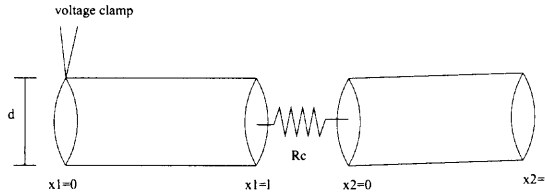
Figure 3.1 The two cables are electrically end-to-end coupled with diameter d and coupling resistance R_c.

We study the voltage response of gap junctionally coupled cables as a function of cable diameter. We have obtained the following results:

1. For any non-negative inputs, we show that there exists an optimal diameter for which the maximum voltage response of the second cable occurs in response to both steady state and transient inputs.

2. We derive the exact form of stationary solutions for gap junctionally coupled cables in response to periodic waves and step voltage clamps.

3. We find a sufficient condition that guarantees the existence of an optimal diameter for any network architecture of multiple gap junctionally cables.

4. We give mathematical explanations for the existence of an optimal diameter in terms of voltage flux.

3.1 Two Gap Junctionally end-to-end Coupled Cables

In this section, we consider two passive cables that are coupled by a gap junction with a periodic wave input. A single linear cable equation is given by [17].

$$\tau_m \frac{\partial v(x,t)}{\partial t} = \lambda^2 \frac{\partial^2 v(x,t)}{\partial x^2} - v(x,t), \tag{3.1}$$

where $v(x,t)$ is the voltage at x at time t, $0 \leq x \leq l$, and $t > 0$, τ_m is the membrane time constant and λ is a space constant of the cable.

For a single cable case, the solution of equation (3.1) can be uniquely determined for any two boundary conditions at $x = 0$ and $x = l$, respectively [18]. For example, a

common situation would be to voltage clamp at $x = 0$, $v(0, t) = v_0(t)$ and to impose a no flux condition at the sealed end, $\frac{\partial v(l,t)}{\partial x} = 0$.

Assume that two identical cables are connected end-to-end by a gap junction with a coupling resistance R_c and that we clamp a voltage at the beginning of the first cable. Then the current flow diffuses along the first cable, crosses the gap junction and then diffuses along the second cable. A coupled model is given by equations (3.2) and (3.3).

$$\tau_m \frac{\partial v_i(x, t)}{\partial t} = \lambda^2 \frac{\partial^2 v_i(x_i, t)}{\partial x_i{}^2} - v_i(x_i, t), \tag{3.2}$$

if $0 \leq x_1 < l, 0 < x_2 \leq l, 0 \leq t$, and $i = 1, 2$,

$$\frac{v_1(l, t) - v_2(0, t)}{R_c} = -\frac{1}{r_a} \frac{\partial v_2(0, t)}{\partial x}, \tag{3.3}$$

where R_c is a coupling resistance. The boundary conditions are

$$v_1(0, t) = v_0(t),$$

$$\frac{\partial v_2(l, t)}{\partial t} = 0.$$

and initial conditions of the coupled system are

$$v_1(x_1, 0) = v_2(x_2, 0) = 0$$

for all $0 \leq x_i \leq l$, $i = 1, 2$.

Nadim and Golowasch determined a steady state voltage response of the two gap junctionally coupled cables in response to a voltage clamp as a function of input amplitude, diameter, coupling resistance, input resistance, terminal resistance, and

diameter [20]. Their main results show that the voltage response at any location of the second cable is maximized at a location dependent optimal diameter.

Note if the two coupled cable equations (3.2) and (3.3) are considered to be a single cable with a gap junction, the voltage response of model $(0 \leq x \leq 2l)$ has a discontinuity at the gap junction location $x = l$. Here we solve each cable equation separately. First, the voltage response along each coupled cable can be expressed as the two unknown voltage fluxes which are determined at $x_1 = l$ for the first cable and $x_2 = 0$ for the second cable, respectively. Second, we derive a matching condition across the gap junction to determine the two unknown fluxes.

We solve the above equations (3.2) and (3.3) using Green's function. An explicit dependency of cable diameter appears in axial resistance r_a and space constant λ where

$$r_a = \frac{4R_a}{\pi d^2}$$

and

$$\lambda = \sqrt{\frac{R_m d}{4R_a}}.$$

Where d is the cable diameter with unit μm and R_a is the axial resistivity with unit $\Omega \cdot cm$ and R_m is the specific membrane resistance with unit $\Omega \cdot cm^2$.

3.2 Derivation of the Solution and a Matching Condition across the Gap Junction

We assume that current does not leak out through the membranes at the proximal and distal ends. Thus the current is conserved through the gap junction, $I_{1a}(l, t) = I_c = I_{2a}(0, t)$, where the current $I_{1a}(l, t)$ flows out at the end of the first cable $(x_1 = l)$, the current $I_{2a}(0, t)$ flows in at the beginning of the second cable $(x_2 = 0)$ and I_c flows across gap junction $(x_1 = l$ and $x_2 = 0)$:

$$-\frac{1}{r_a}\frac{\partial v_1(l,t)}{\partial x_1} = I_{1a}(l,t),$$

$$-\frac{1}{r_a}\frac{\partial v_2(0,t)}{\partial x_2} = I_{2a}(0,t), \tag{3.4}$$

$$\frac{v_1(l,t) - v_2(0,t)}{R_c} = I_c$$

We separate the above discontinuous P.D.E (3.2) and (3.3) by denoting the unknown voltage flux $\frac{\partial v_1(1,t)}{\partial x_1}$ by $a(t)$:

$$\tau_m \frac{\partial v_i(x_i,t)}{\partial t} = \lambda^2 \frac{\partial^2 v_i(x_i,t)}{\partial x^2} - v_i(x_i,t), \quad i = 1,2 \tag{3.5}$$

The initial conditions are

$$v_i(x_i,0) = 0 \quad i = 1,2$$

and the boundary conditions are

$$v_1(0,t) = v_0(t), \quad \frac{\partial v_1(l,t)}{\partial x_1} = a(t),$$

$$\frac{\partial v_2(0,t)}{\partial x_2} = a(t), \quad \frac{\partial v_2(l,t)}{\partial x_2} = 0,$$

for $i = 1,2$ where $a(t)$ is unknown. The corresponding Green's functions of (3.5):

$$G_1(\xi,\tau;x,t) = \frac{\exp(-\frac{(t-\tau)}{\tau_m})}{\sqrt{4\pi\frac{(t-\tau)}{\tau_m}}} \sum_{-\infty}^{\infty}(-1)^n \tag{3.6}$$

$$\left[\exp\left(\frac{-\tau_m(\xi - x - 2nl)^2}{4\lambda^2(t-\tau)}\right) - \exp\left(\frac{-\tau_m(\xi - 2nl + x)^2}{4\lambda^2(t-\tau)}\right)\right]$$

$$G_2(\xi,\tau;x,t) = \frac{\exp(-\frac{(t-\tau)}{\tau_m})}{\sqrt{4\pi\frac{(t-\tau)}{\tau_m}}} \sum_{-\infty}^{\infty} \tag{3.7}$$

$$\left[\exp\left(\frac{-\tau_m (\xi - 2nl - x)^2}{4\lambda^2 (t - \tau)} \right) + \exp\left(\frac{-\tau_m (\xi - 2nl + x)^2}{4\lambda^2 (t - \tau)} \right) \right]$$

G_1 and G_2 are obtained by the method of images. By using integration by parts and the boundary conditions of each cable, the solution can be expressed with an unknown flux $a(t)$.

$$v_1(x_1, t) = \int_0^t G_{1\xi}(0, \tau; x_1, t) v_0(\tau) d\tau + \int_0^t G_1(l, \tau; x_1, t) a(\tau) d\tau \qquad (3.8)$$

$$v_2(x, t) = -\int_0^t G_2(0, \tau; x_1, t) a(\tau) d\tau. \qquad (3.9)$$

From equation (3.4), (3.8) and (3.9)

$$-\frac{R_c}{r_a} a(t) = v_1(l, t) - v_2(0, t). \qquad (3.10)$$

Thus, the discontinuous P.D.E.(3.2) and (3.3) has been reduced to a linear integral equation for the unknown $a(t)$. Note that the only input to the second cable for the equations (3.2) and (3.3) with the given boundary conditions is positive and comes from the end of the first cable. Thus current flows from $x_1 = l$ to $x_2 = 0$. Therefore, we have $a(t) < 0$ throughout this chapter. Substituting (3.8) and (3.9) into (3.10) we obtain

$$
\begin{aligned}
-\frac{R_c}{r_a} a(t) &= \int_0^t G_{1\xi}(0, \tau; l, t) v_0(\tau) d\tau + \int_0^t G_1(l, \tau; l, t) a(\tau) d\tau \\
&+ \int_0^t G_2(0, \tau; x, t) a(\tau) d\tau. \qquad (3.11)
\end{aligned}
$$

Since the infinite series of Green's functions converges very fast for small times, the first few terms of (3.6) and (3.7) can be used to solve the linear integral equation

(3.11). Once we know the voltage flux $a(t)$ from (3.11), the voltage response $v_2(x, t)$ along the second cable is obtained by (3.9). Once we obtain the two Green's functions (3.6) and (3.7), we do not have to calculate them for each value of parameters. That is an advantage to use the integral equation (3.11) rather than solving the problem by direct numerical methods. Note that the linearity of (3.11) can be used to show that $a(t)$ is linear with respect to inputs by using Laplace transformation. This fact is used below.

3.3 Stationary Solution in Response to a Periodic Voltage Clamp

We consider a stationary solution for the boundary conditions:

$$v_1(0, t) = v_0 sin(\omega t)$$

and

$$\frac{\partial v_2(l, t)}{\partial x} = 0.$$

Since the governing equations (3.2) and (3.3) are linear, a complex-valued boundary condition $I_0 exp(i\omega t)$ is applied at the beginning of the first cable rather than $I_0 sin(i\omega t)$ in order to make calculation easier.

We expect that a stationary voltage response of periodic input $v_0 exp(i\omega t)$ has the same frequency as the input frequency w. Thus we assume that the unknown boundary conditions have the form $A exp(i\omega t)$ where A is a constant. So an ansatz $u_j(x) exp(i\omega t)$ is inserted in the equation (3.5) for $j = 1, 2$:

$$i\omega u_j(x) \exp(i\omega t)\tau_m = \lambda^2 u_j^{''}(x) \exp(i\omega t) - u_j(x) \exp(i\omega t), \qquad (3.12)$$

where $' = \frac{d}{dx}$. Then, (3.2) and (3.3) become two boundary value ordinary differential equations with the boundary conditions:

$$u_1(0) = v_0, u_1^{'}(l) = A, u_2^{'}(0) = A \qquad (3.13)$$

and

$$u_2'(l) = 0, \tag{3.14}$$

where A is unknown and to be determined. Rewriting (3.12), we obtain

$$\lambda_\omega{}^2 u_j''(x) - u_j(x) = 0, \tag{3.15}$$

where

$$\lambda_\omega{}^2 = \frac{\lambda^2}{1 + i\omega\tau_m}, \quad j = 1, 2.$$

Across the gap junction, the matching condition must satisfy:

$$-\frac{R_c}{r_a}A = u_1(l) - u_2(0) \tag{3.16}$$

By solving the above two boundary value problems with the matching condition (3.16), we obtain a solution along the second cable:

$$u_2(x) = \frac{v_0}{\frac{R_c}{r_a\lambda_\omega}cosh(\frac{l}{\lambda_\omega})sinh(\frac{l}{\lambda_\omega}) + 2sinh^2(\frac{l}{\lambda_\omega}) + 1}cosh(\frac{l - x}{\lambda_\omega}) \tag{3.17}$$

In the case of $\omega = 0$, $v_1(0, t) = v_0$, the solution $u_2(x)$ is the same as Nadim and Golowasch have obtained in the form of a system of algebraic equations.

3.4 An Optimal Diameter for Voltage Amplitude along the Second Cable

We now use (3.17) to show that there exists an optimal diameter for which the maximum amplitude of the voltage response along the second cable can be achieved. First, define a new space constant λ_w of the passive cable model in response to a periodic input $v_0sin(\omega t)$ as:

$$\lambda_\omega = \frac{\lambda}{(1 + i\omega\tau_m)^{\frac{1}{2}}} = \frac{\sqrt{\frac{R_m}{R_a}}}{2(1 + \tau_m^2\omega^2)^{\frac{1}{4}}}e^{(i\alpha)}\sqrt{d},$$

$$\alpha = \frac{1}{2}\tan^{-1}(-\tau_m\omega) \tag{3.18}$$

Our governing model is linear and thus the input $v_0 e^{i\omega t}$ is a linear superposition of $v_0 cos(\omega t)$ and $i v_0 sin(\omega t)$. A true stationary solution of the coupled cables equation along the second cable corresponds to the imaginary part of $u_2(x)e^{i\omega t}$. Even though $u_2(x)$ is a complex-valued function of x, it is still useful to consider the magnitude of $u_2(x)$. The amplitude of stationary voltage response along the second cable in response to $v_0 sin(\omega t)$ is the magnitude of a complex-valued function $u_2(x)$. Note that $u_2(x)$ also depends on ω and d. The phase shift in response to an input $v_0 sin(\omega t)$ along coupled cable is $arg(u_2(x))$. To see this, denote $u_2(x)$ by $v(x) + iw(x)$. Then

$$u_2(x)e^{i\omega t} = vcos(\omega t) - wsin(\omega t) + i(wcos(\omega t) + vsin(\omega t)).$$

$$imag(u_2(x)e^{i\omega t}) = wcos(\omega t) + vsin(\omega t) = \sqrt{v^2 + w^2}sin(\omega t + \phi)$$

where $tan(\phi) = \frac{w}{v}$. Define the phase shift of input $v_0 sin(\omega t)$ along coupled cable as ϕ. Then $\phi = arg(u_2(x))$.

In this section, we investigate the effects of parameters d and ω on the amplitude of the voltage response. First we understand the effect of d on the amplitude. When u_2 is considered to be a function of d, we show that there exists an optimal diameter for which the maximum amplitude of the stationary voltage response can be obtained. In Figure 3.2, we plot $|u_2(x)|$ versus d using the equation (3.17). The amplitude of the voltage response along the second cable can be optimized at $d = d^* \approx 3.2$ for the set of parameters shown.

Theorem 3.4.1 Fix ω and consider a fixed location x_2 along the second cable. There exists an optimal diameter $d^*(x_2, \omega)$ where the amplitude of the stationary voltage response is maximized.
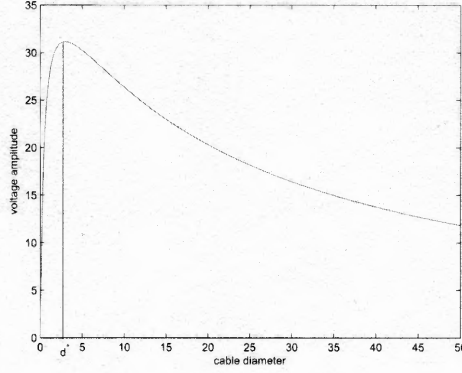
Figure 3.2 The voltage amplitude $|u_2(x)|$ plotted from (3.17) along the second cable is maximized at $d = d^\star \approx 3.2$ where $x_2 = 3, \omega = 5, l = 600\mu m, v_1(0,t) = 40mv, R_m = 40k\Omega cm^2, R_a = 60\Omega cm, R_c = 10^8\Omega$.

Note that we can restate the conclusion of Theorem 3.4.1 simply as $|u_2(x_2, \omega, d)| \leq |u_2(x_2, \omega, d^\star)|$ for any $d \neq d^\star$ and $d > 0$.

Proof of Theorem 3.4.1

Fix x along the second cable and also fix the input frequency ω. From (3.18),

$$\frac{1}{\lambda_\omega} = \frac{K(cos(-\alpha) + isin(-\alpha))}{\sqrt{d}} = \frac{z_0}{\sqrt{d}}$$

where

$$K = 2\sqrt{\frac{R_a}{R_m}}(1 + \tau_m{}^2\omega^2)^{\frac{1}{4}},$$

$$\alpha = \frac{1}{2}\arctan(-\tau_m\omega),$$

$$z_0 = K(cos(-\alpha) + isin(-\alpha)),$$

and

$$\frac{1}{r_a\lambda_\omega} = \frac{\pi}{4R_a}Kd^{\frac{3}{2}}(cos(\alpha) + isin(-\alpha)).$$

From (3.17) and the triangle inequality,

$$|u_2(x)| \leq \frac{|v_0 cosh(\frac{l-x}{\lambda_\omega})|}{\left||\frac{R_c}{r_a \lambda_\omega} cosh(\frac{l}{\lambda_\omega}) sinh(\frac{l}{\lambda_\omega})| - |2sinh^2(\frac{l}{\lambda_\omega}) + 1|\right|}.$$

First, we claim that as d approaches ∞, $|u_2(x)|$ goes to 0. Note that

$$\lim_{d \to \infty} |2sinh^2(\frac{l}{\lambda_\omega}) + 1| = 1$$

and

$$\lim_{d \to \infty} cosh(\frac{l-x}{\lambda_\omega}) = 1$$

since $\frac{l}{\lambda_\omega}$ goes to 0 in the complex plane. But $|\frac{1}{r_a \lambda_\omega} sinh\frac{l}{\lambda_\omega}|$ has an indefinite form $\infty \times 0$ as d goes to ∞. Hence it suffices to show that $|\frac{1}{r_a \lambda_\omega} sinh\frac{l}{\lambda_\omega}|$ approaches ∞ as d goes to ∞.

$$\begin{aligned}
|\frac{1}{r_a \lambda_\omega} sinh\frac{l}{\lambda_\omega}| &= \frac{\pi K}{4R_a} d^{\frac{3}{2}} |sinh(\frac{l}{\lambda_w})| \\
&= \frac{\pi K}{4R_a} d^{\frac{3}{2}} |sinh(\frac{lz_0}{\sqrt{d}})| \\
&= \frac{\pi K}{4R_a} |\frac{sinh(lz_0 t)}{t^3}|
\end{aligned}$$

where $t = \sqrt{d}$. Thus,

$$\lim_{d \to \infty} |\frac{1}{r_a \lambda_\omega} sinh\frac{l}{\lambda_\omega}| = \lim_{t \to 0} \frac{\pi K}{4R_a} |\frac{sinh(lz_0 t)}{t^3}| = \infty.$$

Thus as $d \longrightarrow \infty$, $|u_2(x)| \longrightarrow 0$.

Now, we claim that as d goes to 0, $|u_2(x)|$ tends to 0.

$$|u_2(x)| \leq \left|\frac{v_0 cosh(\frac{l-x}{\lambda_\omega})}{cosh(\frac{l}{\lambda_\omega})}\right| \frac{1}{\left||\frac{R_c}{r_a \lambda_\omega} sinh(\frac{l}{\lambda_\omega}) + 2cosh(\frac{l}{\lambda_\omega})| - \frac{1}{|cosh(\frac{l}{\lambda_\omega})|}\right|}$$

Since $\frac{1}{|cosh(\frac{l}{\lambda_\omega})|}$ approaches 0 as d goes to 0 and

$$|cosh(\frac{l-x}{\lambda_\omega})| \leq |cosh(\frac{l}{\lambda_\omega})|,$$

$$|u_2(x)| \leq \frac{|v_0|}{\left| |\frac{R_c}{r_a\lambda_\omega}sinh(\frac{l}{\lambda_\omega}) + 2cosh(\frac{l}{\lambda_\omega})| - 1 \right|}$$

$$\leq \frac{|v_0|}{\left| |\frac{R_c}{r_a\lambda_\omega}sinh(\frac{l}{\lambda_\omega})| - |2cosh(\frac{l}{\lambda_\omega})| \right| - 1}$$

for a large enough d. Using the complex function identities:

$$sinhz = sinhxcosy + icoshxsiny$$

and

$$coshz = coshxcosy + isinhxsiny$$

for $z = x + iy$, note that

$$|\frac{R_c}{r_a\lambda_\omega}sinh(\frac{l}{\lambda_\omega})| = \frac{R_c\pi k}{4R_a}d^{\frac{3}{2}}|sinh(\frac{l}{\lambda_\omega})|$$

$$= \frac{R_c\pi k}{4R_a}d^{\frac{3}{2}}\sqrt{cosh^2(\frac{lkcos(\alpha)}{\sqrt{d}}) - cos^2(\frac{lksin(\alpha)}{\sqrt{d}})}$$

and

$$|2cosh(\frac{l}{\lambda_\omega})| = 2\sqrt{sinh^2(\frac{lkcos(\alpha)}{\sqrt{d}}) + cos^2(\frac{lksin(\alpha)}{\sqrt{d}})}.$$

Hence,

$$|\frac{R_c}{r_a\lambda_\omega}sinh(\frac{l}{\lambda_\omega})| \quad - \quad |2cosh(\frac{l}{\lambda_\omega})|$$

$$= \frac{R_c\pi k}{4R_a}e^{\frac{lkcos(\alpha)}{\sqrt{d}}}(\frac{d^{\frac{3}{2}}\sqrt{cosh^2(\frac{lkcos(\alpha)}{\sqrt{d}}) - cos^2(\frac{lksin(\alpha)}{\sqrt{d}})}}{e^{\frac{lkcos(\alpha)}{\sqrt{d}}}}$$

$$- \frac{2\sqrt{sinh^2(\frac{lkcos(\alpha)}{\sqrt{d}}) + cos^2(\frac{lksin(\alpha)}{\sqrt{d}})}}{e^{\frac{lkcos(\alpha)}{\sqrt{d}}}}).$$

As d goes to 0, both

$$\frac{\sqrt{cosh^2(\frac{lkcos(\alpha)}{\sqrt{d}}) - cos^2(\frac{lksin(\alpha)}{\sqrt{d}})}}{e^{\frac{lkcos(\alpha)}{\sqrt{d}}}}$$

and

$$\frac{\sqrt{sinh^2(\frac{lkcos(\alpha)}{\sqrt{d}}) + cos^2(\frac{lksin(\alpha)}{\sqrt{d}})}}{e^{\frac{lkcos(\alpha)}{\sqrt{d}}}},$$

approach 1. Thus,

$$|\frac{R_c}{r_a\lambda_\omega}sinh(\frac{l}{\lambda_\omega})| - |2cosh(\frac{l}{\lambda_\omega})| \to -\infty$$

as $d \to 0$. Therefore, $|u_2(x)| \longrightarrow 0$ as $d \longrightarrow 0$. From (3.17), since $|cosh(\frac{l-x}{\lambda_\omega})| > 0$ for any $0 < d < \infty$. By the mean value theorem, there exists an optimal diameter d for which $|u_2(x)|$ can be maximized.

Note that this does not prove the uniqueness of the optimal diameter value, but locally shows that there exists an optimal diameter $d^*(x,\omega)$ such that $|u_2(x,d)| \leq |u_2(x,d^*)|$ for each x and ω. We plotted the imaginary part of $u_2(x)$ versus d for different choice of parameters, as in Figure 3.2. The results suggest that the optimal diameter is in fact unique.

Next, we examine the effects of the input frequencies on the amplitude of voltage. By fixing x_2 along the second cable, we can check how the amplitude $|u_2(x_2)|$ varies as we change ω. In Figure 3.3, we plot $|u_2(x_2)|$ versus ω. The plot certainly suggests that $|u_2(x_2)|$ is monotonically decreasing as is the case of an iso-potential cell [24]. We do not yet have a proof that $|u_2(x)|$ monotonically decreases with ω. But we do have a partial result. We prove that $|u_2(x)| \to 0$ as $\omega \to \infty$.

Theorem 3.4.2 Fix x along the second cable. Then, $|u_2(x)| \to 0$ as $\omega \to \infty$.

Proof of Theorem 3.4.2

$$\frac{l}{\lambda_\omega} = \frac{2\sqrt{\frac{R_a}{R_m}}(1 + \tau_m^2\omega^2)^{\frac{1}{4}}}{d}e^{\frac{1}{2}tan^{-1}(\tau_m\omega)i} \qquad (3.19)$$
$$\equiv A(\omega)e^{\alpha(\omega)i},$$
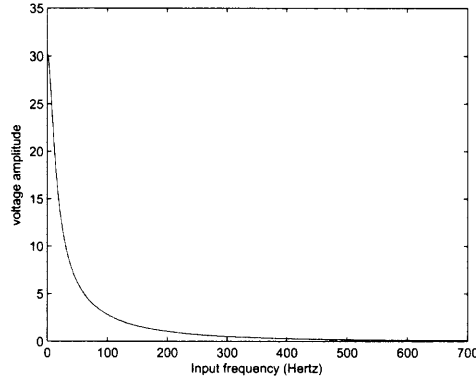
Figure 3.3 As in an iso-potential cell, the voltage amplitude along the second cable decreases to zero as input frequency ω increases where $x_2 = 3, d = 5$.

where $A(\omega) \equiv 2\dfrac{\sqrt{\frac{Ra}{Rm}}(1+\tau_m{}^2\omega^2)^{\frac{1}{4}}}{d}$ and $\alpha(\omega) \equiv \frac{1}{2}tan^{-1}(\tau_m\omega)$

$$|u_2(x)| = \frac{|v_0|}{|\frac{R_c}{r_a\lambda_\omega}cosh(\frac{l}{\lambda_\omega})sinh(\frac{l}{\lambda_\omega}) + 2sinh^2(\frac{l}{\lambda_\omega}) + 1|}|cosh(\frac{l-x}{\lambda_\omega})|$$

The dominant term is $e^{\frac{2l}{\lambda_\omega}}$ and divide the numerator and denominator by $|e^{\frac{2l}{\lambda_\omega}}|$.

Then,

$$|u_2(x)| = \frac{|v_0|}{|\frac{1}{e^{\frac{2l}{\lambda_\omega}}}||\frac{R_c}{r_a\lambda_\omega}cosh(\frac{l}{\lambda_\omega})sinh(\frac{l}{\lambda_\omega}) + 2sinh^2(\frac{l}{\lambda_\omega}) + 1|}|cosh(\frac{l-x}{\lambda_\omega})|\frac{1}{e^{\frac{2l}{\lambda_\omega}}}|$$

The real part of $-4(\frac{2l}{\lambda_\omega})$ is $-8A(\omega)cos(\alpha)$. As $\omega \longrightarrow \infty$, $-8A(\omega)cos(\alpha) \longrightarrow -\infty$

since $A(\omega) \longrightarrow \infty$ and $\alpha \longrightarrow \frac{\pi}{4}$. Thus, $\lim_{\omega\to\infty}\frac{cosh(\frac{l}{\lambda_\omega})sinh(\frac{l}{\lambda_\omega})}{e^{\frac{2l}{\lambda_\omega}}} = \frac{1}{4}$ in the complex

plane. Similarly, $(2sinh^2(\frac{l}{\lambda_\omega}) + 1)\frac{1}{e^{\frac{2l}{\lambda_\omega}}}$ goes to 1 in the complex plane as $\omega \longrightarrow \infty$.

The numerator term $cosh(\frac{l-x}{\lambda_\omega})\frac{1}{e^{\frac{2l}{\lambda_\omega}}}$ goes to 0. Therefore $|u_2(x)| \longrightarrow 0$ as $\omega \longrightarrow \infty$.

We can obtain the optimal cable diameter where $\frac{\partial|u_2(x)|}{\partial d} = 0$ by a numerical

simulation. Here we plot the voltage amplitude versus d for different coupling lengths.

We observe that the optimal diameter decreases as the coupling resistance R_c increases.
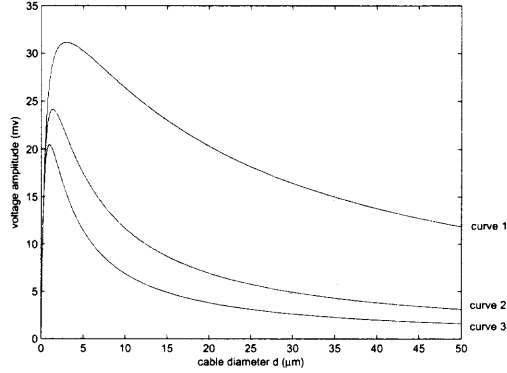
Figure 3.4 The optimal diameter decreases as R_c increases where the curves 1, 2 and 3 are plotted with $R_c = 10^8\Omega, 5 \times 10^8\Omega, 9 \times 10^9\Omega$, respectively, where $x_2 = 3, \omega = 5$.
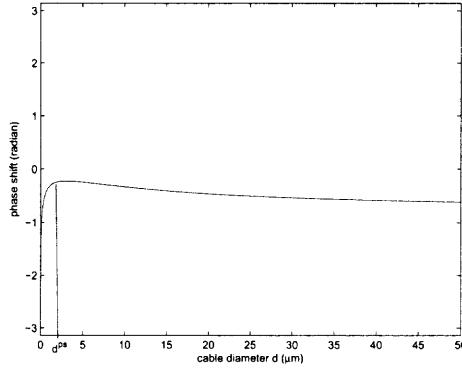
Figure 3.5 The phase shift is minimized at $d = d^{ps} \approx 2.1$ where $x_2 = 3, \omega = 50$.

3.5 Phase Shift as a Function of Diameter

In this section, we observe that for a certain range of ω, there exists an optimal diameter d^{ps} for which the phase shift can be minimized by plotting $arg(u_2(x_2))$ versus d as seen in Figure 3.5. However, for large values of ω, there is no optimal diameter for phase shift because the curve monotonically approaches the limiting value from below as shown in Figure 3.6. For approximately, $\omega > 790$ with choice of parameters of Figure 3.5 and Figure 3.6, there is no optimal diameter for phase shift. In both cases, we find the limiting value of $arg(u_2(x_2))$ as $d \longrightarrow \infty$.
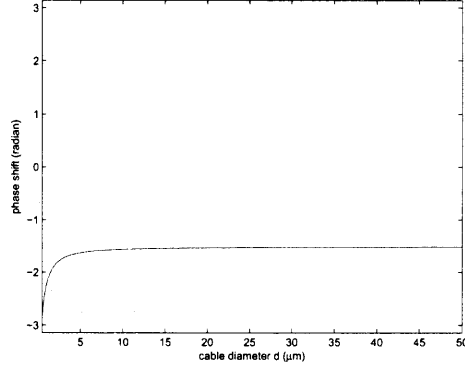
Figure 3.6 The phase shift monotonically approaches the limit value $tan^{-1}(-2\tau_m\omega)$ from below as $d \longrightarrow \infty$. Thus there is no optimal diameter for this frequency where $x_2 = 3, \omega = 800$.

Lemma 3.5.1 $\frac{w}{v} \to -2\tau_m\omega$ as $d \to \infty$ where $u_2(x) = v(x) + iw(x)$.

Proof of Lemma 3.5.1

Rewrite

$$u_2(x) = v_0 \frac{S + iT}{O + 2Q + 1 + i(P + 2R)},$$

where

$$
\begin{aligned}
S &= cosh(\frac{l-x}{\sqrt{d}}A(\omega))cos(\frac{l-x}{\sqrt{d}}B(\omega)), \\
T &= sinh(\frac{l-x}{\sqrt{d}}A(\omega))sin(\frac{l-x}{\sqrt{d}}B(\omega)), \\
O &= \frac{\pi R_c}{4R_a}d^{\frac{3}{2}}\Big(A(\omega)(cosh(\frac{lA}{\sqrt{d}})cos(\frac{lB}{\sqrt{d}})sinh(\frac{lA}{\sqrt{d}})cos(\frac{lB}{\sqrt{d}}) \\
&\quad - sinh(\frac{lA}{\sqrt{d}})sin(\frac{lB}{\sqrt{d}})cosh(\frac{lA}{\sqrt{d}})sin(\frac{lB}{\sqrt{d}})) \\
&\quad - B(\omega)(cosh(\frac{lA}{\sqrt{d}})cos(\frac{lB}{\sqrt{d}})cosh(\frac{lA}{\sqrt{d}})sin(\frac{lB}{\sqrt{d}}) \\
&\quad + sinh(\frac{lA}{\sqrt{d}})sin(\frac{lB}{\sqrt{d}})sinh(\frac{lA}{\sqrt{d}})cos(\frac{lB}{\sqrt{d}}))), \\
P &= \frac{\pi R_c}{4R_a}d^{\frac{3}{2}}\Big(B(\omega)(cosh(\frac{lA}{\sqrt{d}})cos(\frac{lB}{\sqrt{d}})sinh(\frac{lA}{\sqrt{d}})cos(\frac{lB}{\sqrt{d}}) \\
&\quad - sinh(\frac{lA}{\sqrt{d}})sin(\frac{lB}{\sqrt{d}})cosh(\frac{lA}{\sqrt{d}})sin(\frac{lB}{\sqrt{d}}))
\end{aligned}
$$

$$+ \quad A(\omega)(cosh(\frac{lA}{\sqrt{d}})cos(\frac{lB}{\sqrt{d}})cosh(\frac{lA}{\sqrt{d}})sin(\frac{lB}{\sqrt{d}})$$

$$+ \quad sinh(\frac{lA}{\sqrt{d}})sin(\frac{lB}{\sqrt{d}})sinh(\frac{lA}{\sqrt{d}})cos(\frac{lB}{\sqrt{d}}))),$$

$$Q \quad = \quad sinh^2(\frac{lA}{\sqrt{d}})cos^2(\frac{lB}{\sqrt{d}}) - cosh^2(\frac{lA}{\sqrt{d}})sin^2(\frac{lB}{\sqrt{d}}),$$

$$R \quad = \quad 2sinh(\frac{lA}{\sqrt{d}})cos(\frac{lB}{\sqrt{d}})cosh(\frac{lA}{\sqrt{d}})sin(\frac{lB}{\sqrt{d}}),$$

$$A(\omega) \quad = \quad 2\sqrt{\frac{R_a}{R_m}}(1 + \tau_m{}^2\omega^2)^{\frac{1}{4}}cos(\beta),$$

$$B(\omega) \quad = \quad 2\sqrt{\frac{R_a}{R_m}}(1 + \tau_m{}^2\omega^2)^{\frac{1}{4}}sin(\beta), \quad \beta = \frac{1}{2}tan^{-1}(\tau_m\omega).$$

$$(3.20)$$

Separate imaginary and real parts and denote them by $u_2(x) \equiv v + iw$. Then

$$u_2 \quad = \quad \frac{(S + iT)(O + 2Q + 1 - i(P + 2R))}{(O + 2Q + 1)^2 - (P + 2R)^2}$$

$$= \quad \frac{S(O + 2Q + 1) + T(P + 2R) + i(T(O + 2Q + 1) - S(P + 2R))}{(O + 2Q + 1)^2 - (P + 2R)^2}.$$

Thus,

$$\frac{w}{v} = \frac{T(O + 2Q + 1) - S(P + 2R)}{S(O + 2Q + 1) + T(P + 2R)}.$$

Note that

$$\lim_{d \to \infty} S = 1,$$

$$\lim_{d \to \infty} T = \lim_{d \to \infty} Q = \lim_{d \to \infty} R = 0,$$

$$\lim_{d \to \infty} d^{\frac{3}{2}} sinh(\frac{lA}{\sqrt{d}}) = \infty.$$

Hence, O and P are the dominant terms in $\frac{w}{v}$. Thus divide the numerator and

denominator of $\frac{w}{v}$ by $d^{\frac{3}{2}} sinh(\frac{lA}{\sqrt{d}})$. we have

$$\frac{w}{v} = \frac{-S\left(\frac{P}{d^{\frac{3}{2}} sinh(\frac{lA}{\sqrt{d}})} + \frac{2R}{d^{\frac{3}{2}} sinh(\frac{lA}{\sqrt{d}})}\right) + T\left(\frac{O}{d^{\frac{3}{2}} sinh(\frac{lA}{\sqrt{d}})} + \frac{2Q+1}{d^{\frac{3}{2}} sinh(\frac{lA}{\sqrt{d}})}\right)}{S\left(\frac{O}{d^{\frac{3}{2}} sinh(\frac{lA}{\sqrt{d}})} + \frac{2Q+1}{d^{\frac{3}{2}} sinh(\frac{lA}{\sqrt{d}})}\right) + T\left(\frac{P}{d^{\frac{3}{2}} sinh(\frac{lA}{\sqrt{d}})} + \frac{2R}{d^{\frac{3}{2}} sinh(\frac{lA}{\sqrt{d}})}\right)}.$$

Hence, we need to know that $lim_{d\to\infty}\frac{O}{d^{\frac{3}{2}}sinh(\frac{lA}{\sqrt{d}})}$ and $lim_{d\to\infty}\frac{P}{d^{\frac{3}{2}}sinh(\frac{lA}{\sqrt{d}})}$. To do so, check that

$$lim_{d\to\infty}\frac{sin(\frac{lB}{\sqrt{d}})}{sinh(\frac{lA}{\sqrt{d}})} = lim_{z\to0}\frac{sin(lBz)}{sinh(lAz)} = lim_{z\to0}\frac{lBcos(lBz)}{lAcosh(lAz)} = \frac{B}{A}.$$

Thus,

$$lim_{d\to\infty}\frac{O}{d^{\frac{3}{2}}sinh(\frac{lA}{\sqrt{d}})} = \frac{\pi R_c}{4R_a}A - \frac{\pi R_c}{4R_a}\frac{B^2}{A}$$

and

$$lim_{d\to\infty}\frac{P}{d^{\frac{3}{2}}sinh(\frac{lA}{\sqrt{d}})} = \frac{\pi R_c}{4R_a}B + \frac{\pi R_c}{4R_a}B.$$

Finally,

$$lim_{d\to\infty}\frac{w}{v} = -\frac{\frac{\pi R_c}{4R_a}B + \frac{\pi R_c}{4R_a}B}{\frac{\pi R_c}{4R_a}A - \frac{\pi R_c}{4R_a}\frac{B^2}{A}} = \frac{2AB}{B^2 - A^2}$$

$$= \frac{2sin(\beta)cos(\beta)}{sin^2(\beta) - cos^2(\beta)} = -\frac{2sin(2\beta)}{cos(2\beta)}$$

$$= -2tan(2\beta) = -2tan(tan^{-1}(\tau_m\omega))$$

$$= -2\tau_m\omega$$

3.6 An Optimal Diameter for a Transient Solution

We ultimately want to know whether in response to an action potential invoked at the beginning of the first cable, the voltage response at the end of the second cable is above a threshold. To simplify the calculation, we will consider the voltage along the second cable in response to a rectangular potential wave instead of an action potential. We show that in this case, there continues to exist an optimal diameter for voltage. We first show that there exists an optimal diameter of the transient voltage

response of a step voltage clamp in the sense that for fixed x and t, $\frac{\partial v(x,t,d^*)}{\partial d} = 0$ for some d^*. Then we extend the inputs to more general ones including a rectangular potential wave. In this section, we use the properties of cable equation to show the existence of an optimal diameter instead of deriving an analytic form of the transient solution. We now list the properties of cable equation.

Lemma 3.6.1 Let $v(x,t)$ represent the steady state solution of a single cable equation (3.1) with the boundary condition given by $\frac{\partial v(0,t)}{\partial x} \leq 0$ and $\frac{\partial v(l,t)}{\partial x} = 0$. Then $\frac{\partial v(x,t)}{\partial x} \leq 0$ for all $0 < x < l$ and $t > 0$.

Proof of Lemma 3.6.1

Take the derivative (3.1) with respect to x and put $w(x,t) = \frac{\partial v(x,t)}{\partial x}$. Then $\tau_m v_{tx} = \lambda^2 v_{xxx} - v_x$ and thus

$$\tau_m w_t = \lambda^2 w_{xx} - w, w(x,0) = 0, w(0,t) \leq 0, w(L,t) = 0.$$

By the maximum principle of parabolic equation [25], $w(x,t)$ can not attain its maximum in the parabolic interior points of $D = [(x,t)|0 < x < L, 0 < t \leq T]$ but will do so on the parabolic boundary $t = 0, 0 \leq x \leq L$ or $x = 0, 0 \leq t \leq T$ or $x = L, 0 \leq t \leq T$ for some finite $T > 0$. Hence, the maximum $w(x,t)$ over the closure of D is 0. Therefore $w(x,t) \leq 0$.

Lemma 3.6.1 implies that the voltage response decreases along the cable for any fixed $t > 0$. A single cable voltage response to a step voltage clamp can be applied to Lemma 3.6.1. The voltage $v(0,t) = v_0$ is fixed and then current flows down the cable. Thus $\frac{\partial v(0,t)}{\partial x} < 0$.

Next, we begin by showing that there exists an optimal diameter even for a single cable in the case of a current-clamp. However, it does not originate from the property of gap junctions [26].

Lemma 3.6.2 Let $v(x,d)$ represent the steady state solution of a single cable equation (3.1) with the current-clamp boundary condition given by $\frac{\partial v(0,t)}{\partial x} = -r_a I_0$

and $\frac{\partial v(l,t)}{\partial x} = 0$. Then there exists a diameter $d^{\star}(x)$ such that for each $0 < x \leq l$, $v(x,d) \leq v(x, d^{\star}(x))$ for any diameter d.

Proof of Lemma 3.6.2 With the above boundary conditions, we obtain $v(x,d) = \frac{\lambda r_a I_0}{sinh(\frac{l}{\lambda})} cosh(\frac{l-x}{\lambda})$ where $\lambda = \sqrt{\frac{4R_m}{R_a}d} \equiv \frac{\sqrt{d}}{k}$. First, we claim that as $d \longrightarrow \infty$, $v(x,d) \longrightarrow 0$. Note that $cosh(\frac{l-x}{\lambda}) = cosh(\frac{k(l-x)}{\sqrt{d}})$ approaches 1 as d goes to ∞ and $\frac{\lambda r_a I_0}{sinh(\frac{l}{\lambda})} = \frac{I_0}{k} \frac{d^{\frac{1}{2}}}{sinh(\frac{lk}{\sqrt{d}})}$. Then,

$$\lim_{d \to \infty} \frac{\lambda r_a I_0}{sinh(\frac{l}{\lambda})} = \lim_{z \to 0} \frac{I_0}{k} \frac{z^3}{sinh(lkz)} = \lim_{z \to 0} \frac{I_0}{k} \frac{3z^2}{lkcosh(lkz)} = 0.$$

Hence, $\lim_{d \to \infty} v(x,d) = 0$. Now,

$$\lim_{d \to 0} v(x,d) = \lim_{d \to 0} \frac{\lambda r_a I_0}{sinh(\frac{l}{\lambda})} cosh(\frac{l-x}{\lambda}) = \lim_{t \to \infty} \frac{I_0}{k} \frac{t^3(e^{k(l-x)t} + e^{-k(l-x)t})}{e^{klt} - e^{-klt}} = 0$$

for $0 < x$. Thus $\lim_{d \to 0} v(l,d) = 0$. Since $v(x,d) > 0$ for any d, by the mean value theorem, there exists an optimal diameter $d^{\star}$ for which $\frac{\partial v(x,d^{\star})}{\partial d} = 0$.

We can weaken the boundary condition $\frac{\partial v(0,t)}{\partial x} = -r_a I_0$ at $x = 0$ in the sense that $\frac{\partial v(0,t)}{\partial x}$ is bounded by $\frac{K}{d^{\frac{\alpha}{2}}}$ $\alpha > 2$, $K > 0$.

Corollary 3.6.3 If $0 \geq \frac{\partial v(0,t)}{\partial x} \geq \frac{A(t)}{d^{\frac{\alpha}{2}}}$, $\alpha > 2$ in Lemma 3.6.2 where $A(t)$ is independent of d and $A(t) \longrightarrow A$ as $t \longrightarrow \infty$, then there exists an optimal diameter $d^{\star}$ such that for each $0 < x \leq l$, $\frac{\partial v(x,d^{\star})}{\partial d} = 0$.

Proof of Corollary 3.6.3

It is clear that $v(x,d) \leq \frac{\lambda A \frac{1}{d^{\frac{\alpha}{2}}}}{sinh(\frac{l}{\lambda})} cosh(\frac{l-x}{\lambda})$ from the Proof of Lemma 3.6.2. Then

$$\lim_{d \to \infty} \frac{\lambda A \frac{1}{d^{\frac{\alpha}{2}}}}{sinh(\frac{l}{\lambda})} cosh(\frac{l-x}{\lambda}) = 0$$

in the same way in Lemma 3.6.2 since $\alpha > 2$. Thus $\lim_{d \to \infty} v(x,d) = 0$. As $d \to 0$, $v(x,d)$ goes to 0 for any $\alpha > 0$.

Now we claim that the steady voltage response attenuates along the cable.

Lemma 3.6.4 Let $v(x, d)$ represent the steady state solution of a single cable equation (3.1) with the voltage-clamp boundary condition given by $v(0, t) = v_0$ and $\frac{\partial v(l,t)}{\partial x} = 0$. Then $v(x, d) \leq v_0$ for any $x > 0$ and d. Furthermore, $\lim_{d \to \infty} v(x, d) = v_0$ and $\lim_{d \to 0} v(x, d) = 0$.

Proof of Lemma 3.6.4

We obtain $v(x, d) = v_0 \frac{cosh(\frac{l-x}{\lambda})}{cosh(\frac{l}{\lambda})}$ with the two boundary conditions, $v(0, t) = v_0$ and $\frac{\partial v(l,t)}{\partial x} = 0$. It is obvious from the solution that $v(x) \leq v_0$ because $cosh(\frac{l-x}{\lambda}) \leq cosh(\frac{l}{\lambda})$ for all x. Then $\lim_{d \to \infty} v(x) = v_0$ and $\lim_{d \to 0} v(x) = 0$ follow since $\lambda = \frac{\sqrt{d}}{k}$.

Thus in the voltage clamp case, a single cable does not support an optimal diameter. We compare the steady state solution and a transient solution for a single cable in both cases of a current clamp.

Lemma 3.6.5 Let $v(x, t, d)$ represent the transient solution of a single cable equation (3.1) with the current-clamp boundary condition given by $\frac{\partial v(0,t)}{\partial x} = -r_a I_0$ and $\frac{\partial v(l,t)}{\partial x} = 0$. Then $\frac{\partial v(x,t)}{\partial t} > 0$.

Proof of Lemma 3.6.5

Take the derivative of (3.1) with respect to t and put $w(x, t) = \frac{\partial v(x,t)}{\partial t}$. Then $\tau_m v_{tt} = \lambda^2 v_{xxt} - v_t$ and thus

$$\tau_m w_t = \lambda^2 w_{xx} - w, \quad w_x(0, t) = 0, \quad w_x(L, t) = 0. \tag{3.21}$$

Since $v(x, t) \geq 0$ from (3.7) and (3.9) and $v(x, 0) = 0$, the initial conditions $v_t(x, 0) \equiv w(x, 0) \geq 0$. Again by (3.7), (3.9) and the positive contribution to the solution from the initial conditions, $w(x, t) \geq 0$. Thus $v_t(x, t) \geq 0$, which also implies $v(x, t) \leq v(x, d)$ for any $t > 0$.

From Lemma 3.6.2 and Lemma 3.6.5, we immediately figure out the existence of an optimal diameter $d^\star(x, t)$ of the transient solution for a single current clamp cable in the sense that for fixed $x > 0$ and $t > 0$, $\frac{\partial v(x,t,d^\star)}{\partial d} = 0$. Note that $d(x, t)$ depends on x and t.

Corollary 3.6.6 Let $v(x, t, d)$ be the transient solution of a single cable equation (3.1) with the current-clamp boundary condition given by $\frac{\partial v(0,t)}{\partial x} = -r_a I_0$ and $\frac{\partial v(l,t)}{\partial x} = 0$. Then for fixed x and $t > 0$, there exists an optimal diameter $d^\star(x, t)$ such that $v(x, t, d) \leq v(x, t, d^\star(x, t))$ for any d.

Here we compare a transient solution of a single cable with a transient solution of coupled cables at $x_1 = l$ and $x_2 = 0$.

Lemma 3.6.7 If $v_1(x_1, t, d)$ and $v_2(x_2, t, d)$ are the voltage responses of the two end-to-end gap junctionally coupled cables (3.2) and (3.3), $v_1(0, t, d) = v_0$ and $\frac{\partial v_2(l,t,d)}{\partial x} = 0$, then $v_2(0, t, d) \leq v_1(l, t, d) \leq v(l, t, d)$ where $v(l, t, d)$ is the transient voltage response at $x = l$ of a single voltage clamp cable, $v(0, t) = v_0$ and $\frac{\partial v(l,t)}{\partial \partial x} = 0$.

Proof of Lemma 3.6.7 Define $z(x, t, d) = v(x, t, d) - v_1(x, t, d)$. We show $z(x, t, d) \geq 0$ for any x and t with the boundary conditions and initial conditions given by

$$\tau_m \frac{\partial z}{\partial t} = \lambda^2 \frac{\partial^2 z}{\partial x^2} - z, \quad z(x, 0) = 0, \quad z(0, t) = 0, \quad \frac{\partial z(l, t)}{\partial x} = -a(t) > 0.$$

First we claim that $z(l, t) \geq 0$ for all $t > 0$. Suppose $z(l, T) < 0$ for some $T > 0$. Moreover, without loss of generality, assume that $z(l, T)$ is the minimum value in $0 \leq t \leq T$. The minimum principle of the parabolic equation, $z(0, t) = 0$ and $z(x, 0) = 0$ implies that the minimum value of $z(x, t)$ in $[0, l] \times [0, T]$ is $z(l, T)$, which contradicts $z_x(l, T) > 0$. Hence $z(l, t) \geq 0$. Again by the minimum principle of the parabolic equation, $z(x, t) \geq 0$. Since $a(t) < 0$, $v_2(0, t) < v_1(l, t)$. Finally, we combine the above results to show the main result.

Theorem 3.6.8 There exists an optimal diameter $d^\star(x, t)$ for which $v_2(x, t)$ can be maximized along the second cable for fixed $0 \leq x \leq l$ and $t > 0$ in the case of $v_1(0, t) = v_0$ and $\frac{\partial v_2(l,t)}{\partial x} = 0$.

Proof of Theorem 3.6.8

By Lemma 3.6.7 and Lemma 3.6.4, $0 \geq \frac{\partial v_2(0,t)}{\partial x} = -r_a \frac{v_1(l,t)-v_2(0,t)}{R_c} \geq -r_a \frac{v_0}{R_c}$.

From Corollary 3.6.6, for fixed $0 \leq x \leq l$ and $t > 0$, there exists an optimal diameter $d^\star(x,t)$ such that $\frac{\partial v_2(x,t)}{\partial d} = 0$.

An optimal diameter in case of any non-negative input is now considered. A given non-negative input can be bounded by a step voltage clamp. Thus for fixed x and t, the voltage response is bounded by that of the step voltage clamp because the coupled cables model (3.2) and (3.3) are linear with respect to inputs.

Corollary 3.6.9 For any input $v(0,t) = v_0(t) \geq 0$, we can choose a step voltage clamp $V_0 \geq v_0(t)$ for any $t > 0$. Thus there exists an optimal diameter for the voltage response in response to $v_0(t)$.

Proof of Corollary 3.6.9

Since $V_0 \geq v_0(t)$ for any $t > 0$ and the equations (3.2) and (3.3) is linear with respect to input, the voltage response of $v_0(t)$ is less than that of a step voltage clamp. Thus there exists an optimal diameter.

We can extend the existence of an optimal diameter for the two end-to-end gap junctionally coupled cables to a more general case in a network of gap junctionally coupled cables. The proof of Theorem 3.6.10 is obvious.

Theorem 3.6.10 Suppose that $v(x,t)$ is the voltage response along a section of a network of gap junctionally coupled cables. If the voltage flux at the proximal end from the input is bounded by $\frac{K}{d^\alpha}$ where $\alpha > 1$, $K > 0$ and the voltage flux at the distal end is non-positive, then there exists an optimal diameter for which $v(x,t)$ can be maximized along the section of network for fixed x and t.

Example 3.6.11 When two cables are gap-junctionally connected in a middle position, there still exists an optimal diameter for which the voltage response along the second cable can be maximized.

As seen in Figure 3.7, the second cable is separated into the two sections, $0 \leq x_2 \leq l - a$ and $l - a \leq x_2 \leq l$ where a, as measured from the beginning of the first
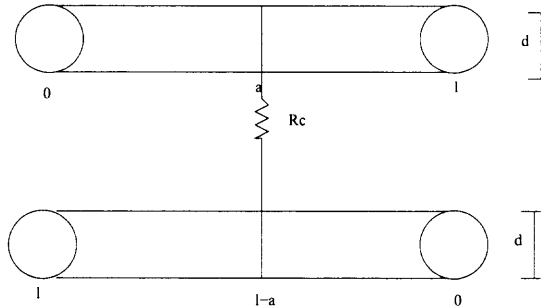
Figure 3.7 A gap junction is located in the middle of the cables which still has the existence of an optimal diameter.

cable, is the gap junction location between the two cables. Assume each end of the second cable is sealed-end, $\frac{\partial v_2(0,t)}{\partial x_2} = \frac{\partial v_2(l,t)}{\partial x_2} = 0$. Denote the two voltage fluxes at $x_2 = (l-a)^+$, $x_2 = (l-a)^-$ by $A(t)$, $B(t)$, respectively. Note that $A(t) \leq 0$ and $B(t) \geq 0$. By the current conservation across the gap location, $\frac{v_1(a,t)-v_2(a,t)}{R_c} = -\frac{A(t)}{r_a} + \frac{B(t)}{r_a}$. Then $-A(t) + B(t) = \frac{r_a}{R_c}(v_1(a,t) - v_2(l-a,t))$. Note that $v_2(l-a,t) \leq v_1(a,t) \leq v_0$, $-A(t) \geq 0$ and $B(t) \geq 0$. Thus $-A(t) \leq r_a\frac{v_0}{R_c}$ and $B(t) \leq r_a\frac{v_0}{R_c}$. Thus $0 \geq A(t) \geq -r_a\frac{v_0}{R_c}$ and $0 \leq B(t) \leq r_a\frac{v_0}{R_c}$. Hence if we consider the two sections of the second cable, the voltage fluxes at the proximal ends are $A(t)$ and $B(t)$, respectively, which are bounded by $\frac{K}{d^2}$. By Theorem 3.6.10, there exists the optimal diameters for the two sections.

3.7 Conclusion

The electrotonic distance is proportional to $\frac{1}{\sqrt{d}}$ and $v_x(x,t) < 0$. When the voltage is clamped at the beginning of a cable, the voltage response of a single cable just monotonically increases at a fixed location as d increases. However, for a current clamp case, the boundary condition at $x = 0$ is $v_x(0,t) = -r_a I_0$ that is bounded by $\frac{K}{d^2}$. As d increases, the input decreases, which allows the voltage response to decrease. However, the electrotonic distance also decreases, which allows the voltage response to increase. Thus there exists an optimal value d for which the voltage response can

be maximized. However, for a voltage clamp case, the input is independent of d and the electrotonic distance only decreases. So the voltage response just monotonically increases as d increases. Throughout several results in Section 3.6, the boundary conditions at $v_{2x}(0,t)$ is bounded by $\frac{1}{d^2}$ in the case of two coupled cables, which guarantees an optimal diameter for the voltage response. Furthermore, given any gap junctionally coupled networks, whether or not there exists an optimal diameter along any section of networks can be determined by knowing the voltage flux at the proximal end of the section from the input.

The results of this chapter show that attenuation of signals in gap-junctionally coupled passive cables can be minimized at a specific cable diameter. The results suggest that neurons may regulate their growth such that their diameters lie in a neighborhood of the optimal diameter, thereby enhancing their ability to transmit action potentials. We also demonstrated that the phase shift in response to sinusoidal inputs can be minimized with respect to diameter. This finding has implications for the arrival timing of inputs to a cable coming from two separate cables. It remains an open question of how we extend these results to neuronal structures that may include active soma and axons.

Gansert et al. numerically show that the propagation along the coupled cables can be minimized around the optimal diameter for voltage amplitude [19]. For a given threshold, from the formula (3.17), there exists an open interval of diameters such that the voltage response for the diameter values of the interval reaches the threshold in a finite time. Since a numerical simulation suggests the voltage flux $a'(t) < 0$ at the gap location, the shortest propagation time presumably occurs at the interval of diameters because the voltage for the diameters outside the interval do not reach the threshold, which is consistent with Gansert et al. work. But the optimal diameter for the steady state voltage does not necessarily support the optimal diameter for the shortest propagation time. In a neighborhood of the voltage optimal diameter, a

numerical simulation shows that the voltage response for a diameter larger than the optimal one reaches the threshold first. This can be explained as follows. Divide the cable equation (3.1) by λ^2. Then for large values of diameters, $\frac{v(x,t)}{\lambda^2}$ can be neglected since λ^2 is proportional to d. So $\frac{\tau_m}{\lambda^2}$ plays a role in a new time constant which is very small. Thus the voltage for the large values of diameter reaches the threshold fast if the corresponding steady state voltage response is above the threshold. However, it again remains an open question to prove this mathematically.

CHAPTER 4

THE DYNAMICS OF ELECTRICALLY COUPLED MODEL
THETA NEURONS

A model of two electrically coupled theta neurons will be introduced. We will provide a geometric phase space description of the dynamics. We study a wide range of conductance values between the two electrically coupled model theta neurons. For a relatively small conductance values, there are several types of solutions (suppressed, 1:multiple, 1:1 solutions) that depend on the uncoupled model theta neurons parameters. For a large conductance, there is a stable 1:1 spiking solution which is independent of the corresponding uncoupled system parameters, as long as there are no fixed points of the system. Due to slow time evolution around origin, the uncoupled system might have a river which is a trajectory that attracts all other trajectories in a certain region in phase space. It can be used to estimate potential river properties for the coupled system.

In this chapter, we will

1. Describe the two dimensional phase space associated with two gap junctionally coupled theta neurons.

2. Utilize Denjoy's Theorem on circle maps to categorize the dynamics of the network.

3. Geometrically construct several of the solutions found by Denjoy's Theorem including $1 : N$ solutions in which one neuron fires once for every N spikes of the other, allowing us to address their stability.

4.1   Geometric Set up of Problem

The theta neuron model is a canonical type I neural oscillator:

$$\theta' = 1 - cos\theta + I(1 + cos\theta), \tag{4.1}$$

where I is an injected current. Note that when $I < 0$, (4.1) has two fixed points between -π and π and when $I > 0$, there are no fixed points and $\theta' > 0$. In this case the phase θ monotonically increases. In order for (4.1) to have an oscillation, we reset the θ value with -π when θ approaches π from below. When we reset, we say that the θ neuron has spiked. When two theta neurons are electrically coupled, the equations become

$$\theta_1' = 1 - cos(\theta_1) + I_1(1 + cos(\theta_1)) - g_c H(\theta_1, \theta_2) \equiv F(\theta_1, \theta_2),$$

$$\theta_2' = 1 - cos(\theta_2) + I_2(1 + cos(\theta_2)) + g_c H(\theta_1, \theta_2) \equiv G(\theta_1, \theta_2), \tag{4.2}$$

where $H(\theta_1, \theta_2) = \theta_1 - \theta_2$ or $H(\theta_1, \theta_2) = sin(\theta_1 - \theta_2)$.

We first consider the case of $H(\theta_1, \theta_2) = \theta_1 - \theta_2$. We analyze the system (4.2) in the phase space $[-\pi, \pi] \times [-\pi, \pi]$.

The θ_1 nullcline is found by setting the RHS of the first equation of (4.2) to 0 and solving for θ_2.

$$\theta_2 = \frac{1}{g_c}(g_c\theta_1 - 1 + cos(\theta_1) - I_1(1 + cos(\theta_1))) \equiv f(\theta_1) \tag{4.3}$$

To find extreme points, we solve $\frac{\partial f(\theta_1)}{\partial \theta_1} = 1 - \frac{1}{g_c}sin(\theta_1) + \frac{I_1}{g_c}sin(\theta_1) = 0$, to obtain

$$sin(\theta_1) = \frac{g_c}{1 - I_1} \tag{4.4}$$
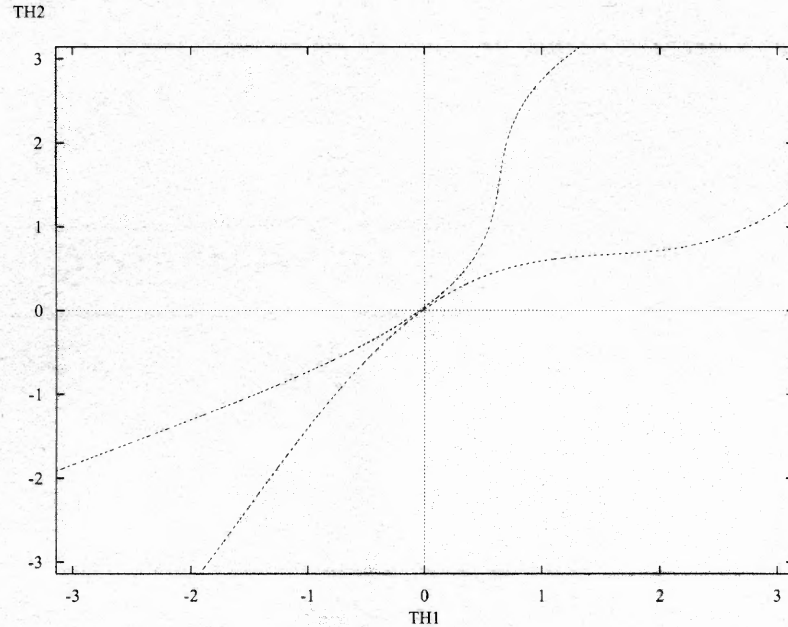
Figure 4.1 The lower curve is the θ_1 nullcline that does not have any extreme points and the upper curve is the θ_2 nullcline where $I_1 = -0.01$, $I_2 = 0.02$, $g_c = 1.1$.

For fixed g_c and I_1, there exists two solutions of (4.4) denoted by $\theta_1^\star$ ($\theta_1^\star < \frac{\pi}{2}$) and $\pi - \theta_1^\star$ if $0 < \frac{g_c}{1-I_1} < 1$. Note that the shape of the θ_1 nullcline depends on its own parameter I_1 and coupling strength g_c, but is independent of I_2. The parameters dependence of the θ_2 nullcline is similar to that of θ_1. There are several properties of the nullclines to consider, depending on the parameters g_c and I_1.

We now list several properties of the nullclines.

Property 1: When $\frac{g_c}{1-I_1} > 1$, there is no extreme point for (4.3). Then the θ_1 nullcline is a strictly monotonic function of θ_1. For fixed I_1, it holds for large values of g_c (see Figure 4.1).

Property 2: When $\frac{g_c}{1-I_1} \leq 1$ and $-\pi \leq f(\theta_1^\star)$, $f(\pi - \theta_1^\star) \leq \pi$, there are two extreme points in the phase space $[-\pi, \pi] \times [-\pi, \pi]$ (see Figure 4.2). This occurs for intermediate values of g_c.
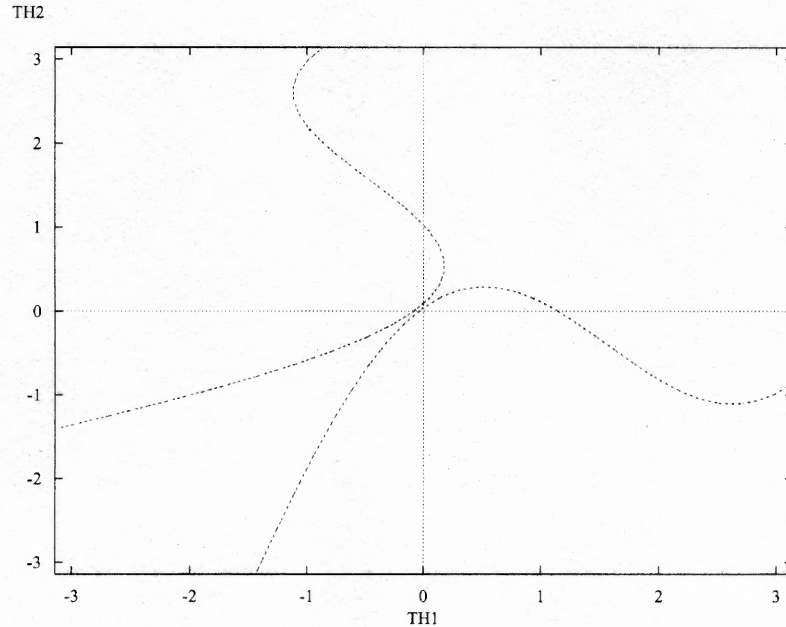
Figure 4.2 The lower curve is the θ_1 nullcline that has the two extreme points and the upper curve is the θ_2 nullcline where $I_1 = -0.01$, $I_2 = 0.02$, $g_c = 0.5$.

Property 3: When $\frac{g_c}{1-I_1} < 1$ and $f(\pi - \theta_1^\star) < -\pi$, then $\theta_1^\star$ is the only extreme point in the phase space $[-\pi, \pi] \times [-\pi, \pi]$. This occurs for small values g_c (see Figure 4.3.

By symmetry, these cases also occur for the θ_2 nullcline and depend on g_c and I_2.

Property 4: When $I_1(I_2)$ increases for Properties 1-3, then the $\theta_1(\theta_2)$ nullcline moves down (left) with an increase of its extreme point $\theta_1^\star = sin^{-1}\frac{g_c}{1-I_1}$.

Property 5: For fixed $I_1 < 0 (I_2 < 0)$ in case of Property 3, the $\theta_1(\theta_2)$ nullcline moves down (left) and spreads out to become tangent to the line $\theta_1 = \theta_2$ as g_c increases. In other words, as g_c increases, the θ_1 nullcline transitions from Property 3 to Property 2, to Property 1, before finally becoming tangent to the line $\theta_1 = \theta_2$ from above (see Figure 4.1-3).
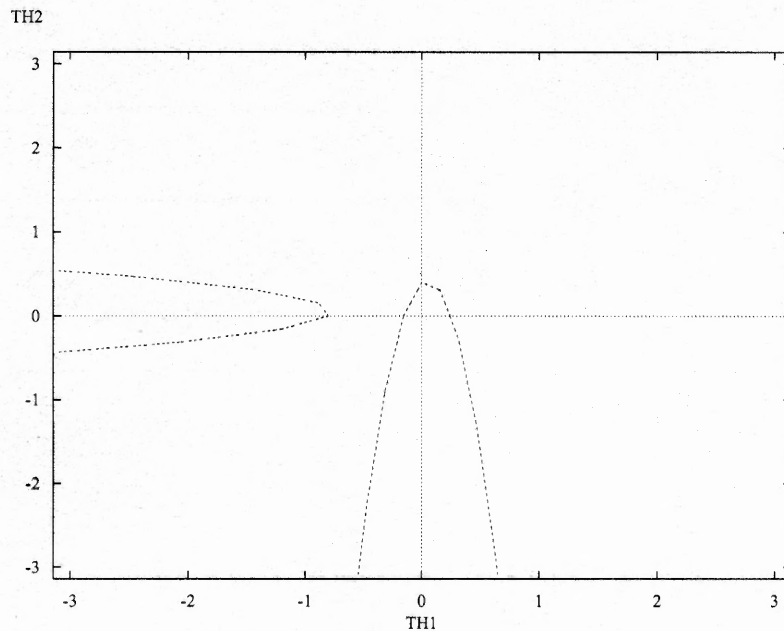
Figure 4.3 The lower curve is the θ_1 nullcline that has the only one extreme point and the upper curve is the θ_2 nullcline where $I_1 = -0.01$, $I_2 = 0.02$, $g_c = 0.05$.
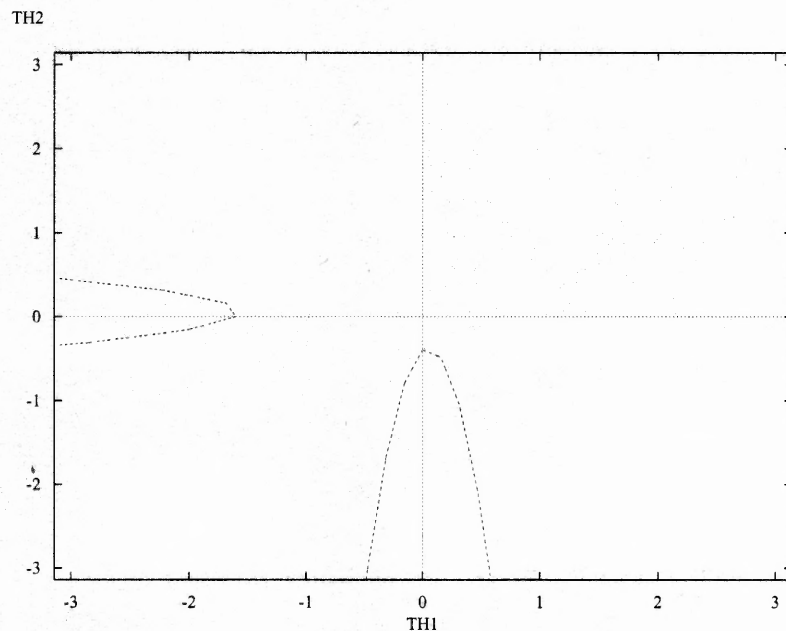
Figure 4.4 The $\theta_1(\theta_2)$ nullcline moves down (left) compared to Figure 4.3 where $I_1 = 0.01$, $I_2 = 0.04$, $g_c = 0.05$.
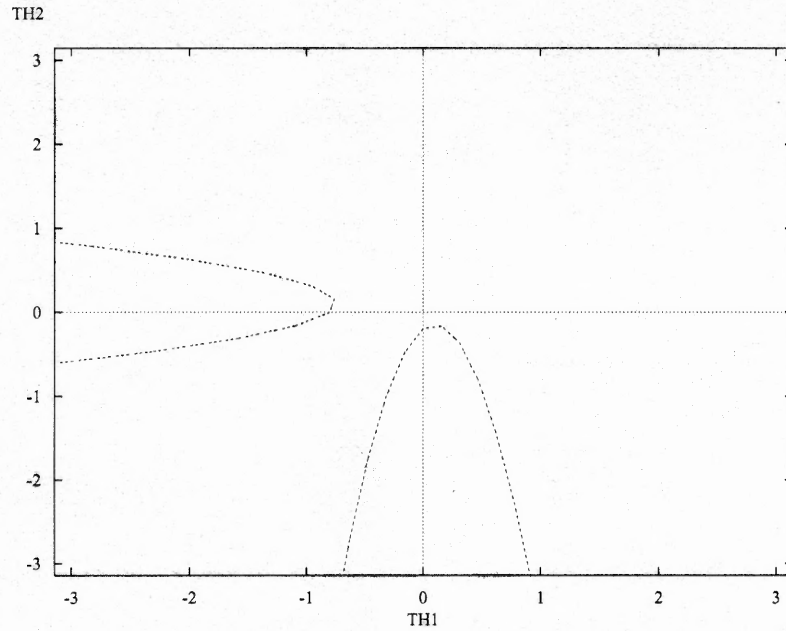
Figure 4.5 The $\theta_1(\theta_2)$ nullcline moves down (right) with spreading out compared to Figure 4.4 where $I_1 = 0.01$, $I_2 = 0.04$, $g_c = 0.1$.
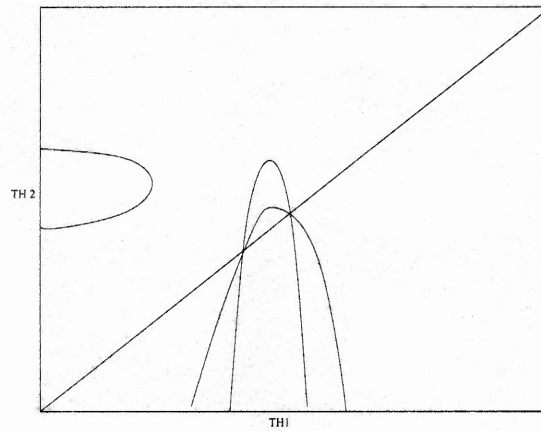
Figure 4.6 The θ_1 nullclines for different values of g_c intersect with the line $\theta_1 = \theta_2$ and the intersection points are independent of g_c.
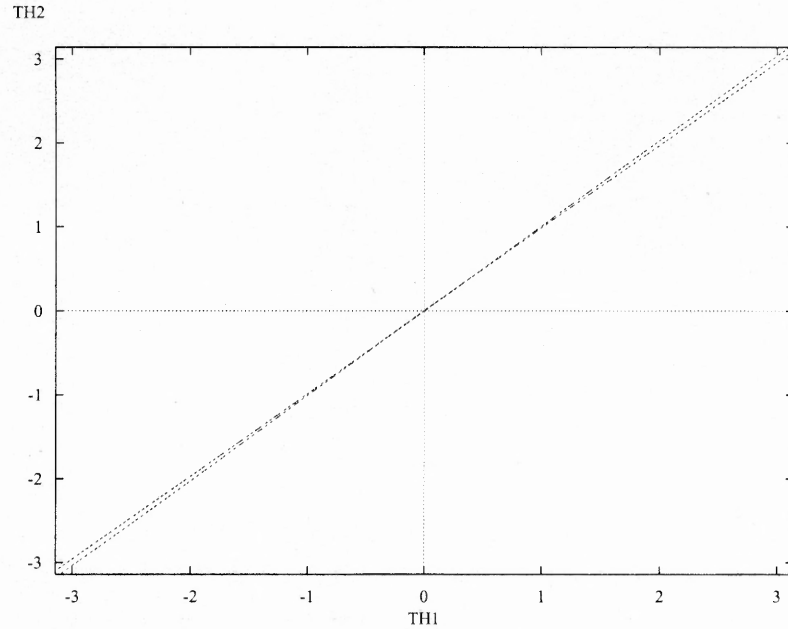
Figure 4.7 The θ_1 and (θ_2) nullcline become tangent to the line $\theta_1 = \theta_2$ where $I_1 = 0.01$, $I_2 = 0.02$, $g_c = 50$.

Property 6: For fixed $I_1 > 0(I_2 > 0)$ in case of Property 3,the $\theta_1(\theta_2)$ nullcline moves up (right) and spreads out to become tangent to the line $\theta_1 = \theta_2$ as g_c increases. In other words, as g_c increases, the θ_1 nullcline transitions from Property 3 to Property 2, to Property 1, before finally becoming tangent to the line $\theta_1 = \theta_2$ from below.

Property 7: For fixed $I_1 < 0(I_2 < 0)$ as in case of Property 5, the $\theta_1(\theta_2)$ nullcline intersects with the line $\theta_1 = \theta_2$ at two points, independent of g_c (Figure 4.6).

In summary, as g_c increases, the θ_1 nullcline moves down and become tangent to $\theta_1 = \theta_2$ from above, but only for negative values of I_1. However, as g_c decreases, the θ_1 nullcline moves up and become tangent to the line $\theta_2 = \pi$ again only for negative values of I_1. For positive values of I_1, the θ_1 nullcline moves up and become tangent to the line $\theta_1 = \theta_2$ as g_c increases but the θ_1 nullcline moves down and disappears from the phase space as g_c decreases. On the other hand, for fixed g_c as I_1 increases, the θ_1 nullcline moves down to disappear from the phase space.
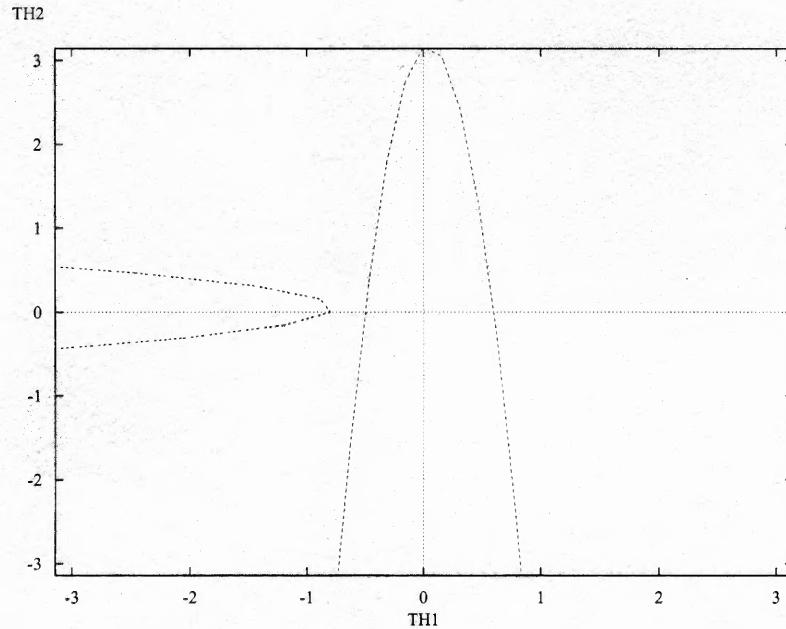
Figure 4.8 The θ_1 nullcline is tangent to the line $\theta_2 = \pi$ at $\theta_1 = \theta_1{}^\star$ where $I_1 = -0.079$, $I_2 = 0.02$, $g_c = 0.05$.

Property 8: For fixed $g_c > 0$ as in Property 3, there exists $I_1 = I_1{}^{top}(g_c)$ such that the θ_1 nullcline is tangent to the line $\theta_2 = \pi$ at the extreme point $\theta_1{}^\star$ (see Figure 4.8). Note that if g_c is fixed, we suppress its dependence in $I_1{}^{top}$.

Property 9: For any given $I_1 < 0$, g_c can be chosen small enough to make the local maximum of the θ_1 nullcline tangent to the line $\theta_2 = \pi$.

When the system (4.2) has the two fixed points, one globally attracts all trajectory in the phase space and the other one is unstable. They disappear through a saddle node bifurcation. Here we do not consider the case. Instead, assume that two nullclines θ_1 and θ_2 do not intersect throughout this paper. This implies that there are no fixed points of the system.

It is valuable to look over the vector field as I_1 varies with fixed I_2 and g_c. In the region where $\theta_1{}' < 0$, $\theta_1{}'$ becomes less negative because $1 + cos(\theta_1) > 0$ as I_1
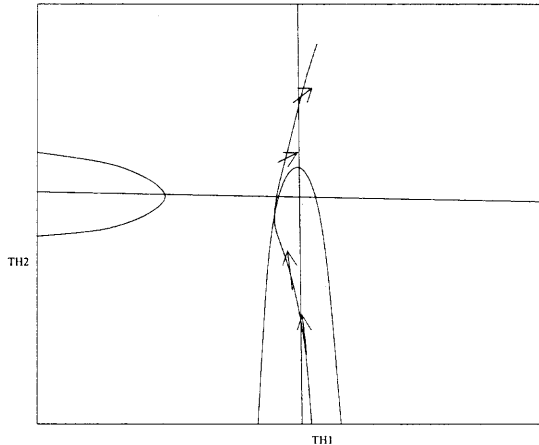
Figure 4.9 The flow for $I_1 = \alpha$ on the curve that is a trajectory for $I_1 = \beta$ points up and and to the right where $\alpha > \beta$.

increases. In the region where $\theta_1' > 0$, θ_1' becomes more positive as I_1 increases. The above can be systematically summarized as follows.

Lemma 4.1.1 If Γ is a trajectory with an initial condition on $\theta_2 = -\pi$ for $I_1 = \alpha$, then the flow on Γ for $I_1 = \beta$, $\alpha < \beta$ points to the right of Γ in the $\theta_1 - \theta_2$ phase space (see Figure 4.10).

Proof of Lemma 4.1.1

Since $\frac{\partial F}{\partial I_1} = 1 + cos(\theta_1) > 0$ and $\theta_2' > 0$, every trajectory starting at the same initial condition as Γ for $I_1 = \beta$ points to the right on Γ.

Now we consider the network of two coupled neurons. We begin with the case $g_c = 0$ to analyze river formation for the uncoupled system. The system (4.2) with $g_c = 0$ yields very interesting trajectories in phase space. The trajectories starting near the $\theta_1(\theta_2)$ axis and $\theta_1 = -\pi(\theta_2 = -\pi)$ moves horizontally(vertically) because the slopes $\frac{\theta_2'}{\theta_1'}$ of the trajectories, except for a neighborhood of the origin, are very small (large) for small $|I_1|$, $|I_2|$ and g_c values (see Figure 4.10).
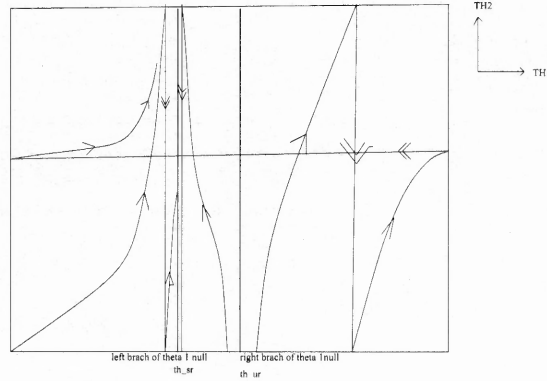
Figure 4.10 The trajectories around $\theta_1(\theta_2)$ axis move up (right) horizontally (vertically). The left branch of the θ_1 nullcline, θ_{sr}, attracts all other trajectories in the phase space, where $I_1 = -0.01$, $I_2 = 0.02$, $g_c = 0.05$.

We describe how the above trajectories approach a certain trajectory, called a river trajectory [27]. Find the θ_1 nullcline of the system (4.2) with $g_c = 0$ by solving:

$$1 - cos(\theta_1) + I_1(1 + cos(\theta_1)) = 0,$$

where $I_1 < 0$. Denote the two solutions by θ_{sr} and θ_{ur}, respectively, where θ_{sr} corresponds to the stable fixed point of the single theta neuron and θ_{ur} for the unstable one. These points correspond to vertical lines in the $\theta_1 - \theta_2$ phase space (see Figure 4.10). We call them a stable river and an unstable river, respectively. As shown in Figure 4.10, the trajectory starting at $(-\pi, -\pi)$ is attracted to the stable θ_{sr}. Thus once a trajectory falls into the region $-\pi \leq \theta_1 \leq \theta_{sr}$, the trajectory must be attracted into θ_{sr}. A trajectory starting between θ_{sr} and θ_{ur} on $\theta_2 = -\pi$ moves up and to the left due to $\theta_1' < 0$ there. The trajectory also is attracted to the stable river after resetting. Any trajectory starting with $\theta_1 \in (\theta_{ur}, \pi)$ will be reset into the region $[-\pi, \theta_{sr})$ after a θ_1 spike and a θ_2 spike. Therefore, the trajectory $\theta_1 = \theta_{sr}$ is globally stable. Furthermore, we estimate how quantitatively the trajectories is attracted to the stable river when $g_c = 0$.

Lemma 4.1.2 A trajectory of (4.2) with $g_c = 0$ starting at $(-\pi, -a)$, $a > 0$, passes the point $(\theta_{sr} - b, 0)$, where $b > 0$ and satisfies

$$\frac{1}{\sqrt{I_2}} tan^{-1}(\frac{tan\frac{a}{2}}{\sqrt{I_2}}) = \frac{1}{2}\frac{1}{\sqrt{-I_1}}ln(\frac{tan(\frac{\theta_{sr}-b}{2}) - \sqrt{-I_1}}{tan(\frac{\theta_{sr}-b}{2}) + \sqrt{-I_1}}).$$

Proof of Lemma 4.1.2 Integrating the second equation of (4.2) with $g_c = 0$ yields

$$\int_\alpha^\beta \frac{d\theta_2}{1 - cos(\theta_2) + I_2(1 + cos(\theta_2))} = \frac{1}{\sqrt{I_2}}[tan^{-1}\frac{tan\frac{\theta_2}{2}}{\sqrt{I_2}}]_\alpha^\beta$$

for $I_2 > 0$, $-\pi < \alpha < \beta < \pi$ [27]. Substitute $\alpha = -a$ and $\beta = 0$ which yields the left-hand side of (4.2). Substitute $v = tan\frac{\theta_1}{2}$, $I_1 = -k^2$ and integrate,

$$\int \frac{d\theta_1}{1 - cos(\theta_1) + I_1(1 + cos(\theta_1))} = \int \frac{1}{v^2 - k^2}dv$$

$$= \frac{1}{2k}\int(\frac{1}{v - k} - \frac{1}{v + k})dv = \frac{1}{2k}ln|\frac{v - k}{v + k}|.$$

Next, apply the upper limit with $\theta_s r - b$ and lower limit with $-\pi$, which yields the right-hand side of (2.6). Since $\theta_1' > 0$ and $\theta_2' > 0$ in $\theta_1 < \theta_{sr}$, the time it takes for θ_1 to evolve from $\theta_1 = -\pi$ to $\theta_1 = \theta_{sr} - b$ equals the time for θ_2 to evolve from $\theta_2 = -a$ to $\theta_2 = 0$.

Lemma 4.1.3 The trajectory of (4.2) with $g_c = 0$ starting at $(\theta_1, \theta_2) = (-c, -\pi)$, $c > 0$, passes the point $(\theta_1^* - d, 0)$, where $d > 0$ and satisfies

$$\frac{\pi}{2\sqrt{I_2}} = \frac{1}{2\sqrt{-I_1}}[ln(\frac{tan(\frac{\theta_{sr}-d}{2}) - \sqrt{-I_1}}{tan(\frac{\theta_{sr}-d}{2}) + \sqrt{-I_1}}) - ln(\frac{tan(\frac{-c}{2}) - \sqrt{-I_1}}{tan(\frac{-c}{2}) + \sqrt{-I_1}})].$$

The proof of the Lemma is similar to the previous one.

When $g_c > 0$, there is still some region in the phase space where trajectories are attracted. We use the next Lemma to see how the flow of the coupled system depends on g_c.

Figure 4.11 — labels: (−e, 0), (−f, 0), (−a, −3.14159), A trajectory for uncoupled system, (g, −3.14159) backward flow of (−f, 0)
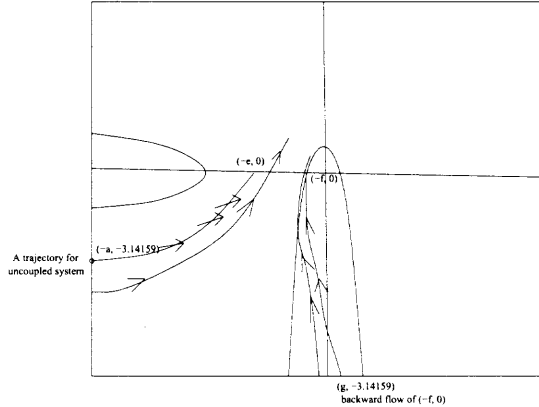
Figure 4.11 Denote the starting and ending points of the uncoupled system by $(-a, \pi)$ and $(-e, 0)$, respectively. Denote also the intersection point of the θ_1 nullcline with the θ_1 axis by $(-f, 0)$. The flow for the uncoupled system points up and to the right. All trajectories starting on $-\pi \times (-\pi, -e)$ or $(-\pi, g) \times -\pi$ are sucked into the interval $(-e, -f)$ where e and f can be calculated from Lemma 4.1.2 and (4.3), respectively.

Lemma 4.1.4 If Γ is a trajectory for $g_c = 0$ starting at $(-\pi, -a)$ for some $a > 0$, then the flow on Γ for $g_c > 0$ and $\theta_2' > 0$ (fixed I_1 and I_2) points to the right of Γ.

Proof of Lemma 4.1.4

The coupling terms $-g_c(\theta_1 - \theta_2)$ and $-g_c(\theta_2 - \theta_1)$ from (4.2) are positive and negative, respectively for $(\theta_1 - \theta_2) < 0$. Therefore, θ_1' become more positive and θ_2' less positive. Therefore the flow points to the right of Γ.

As shown in Figure 4.11, the flow of the coupled system on the trajectory for $g_c = 0$ points to the right. The flow inside the θ_1 nullcline still points up and to the left. Even if the existence of an attracting trajectory, a stable river, for the coupled system is unclear at this moment, trajectories are again sucked into the interval $(-e, -f)$ in the phase space. So we might expect that such a river exists in the coupled system.
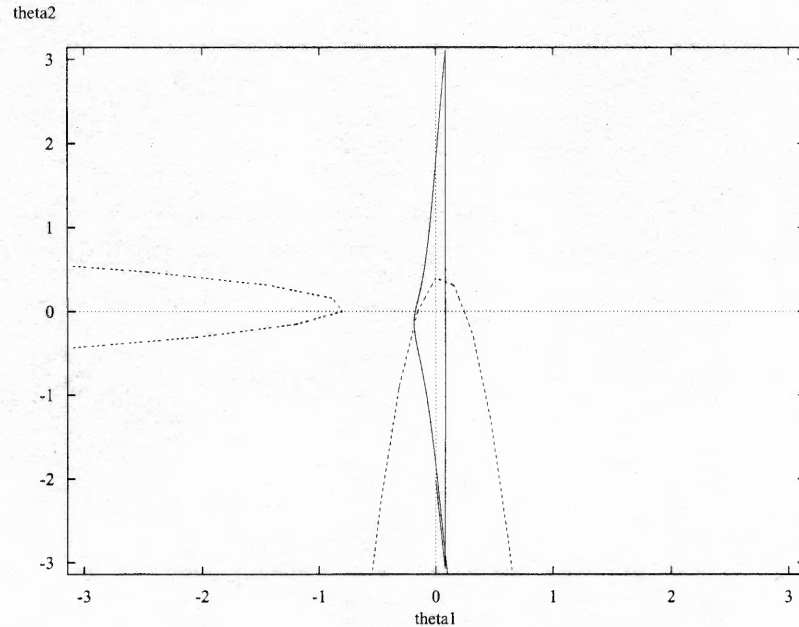
Figure 4.12 The system (4.2) allows a θ_2 spike but not a θ_1 spike where $g_c = 0.05$, $I_1 = -0.01$, $I_2 = 0.02$.

4.2 Suppressed Solution

The trajectory below the θ_1 nullcline moves up and to the left due to $\theta_1' < 0$ and $\theta_2' > 0$. After the trajectory passes through the θ_1 nullcline, the trajectory starts to move up and to the right. When the trajectory starting at a value $\theta_1 = a$ on $\theta_2 = -\pi$ reaches $\theta_2 = \pi$ at time t, we can check the variation in the θ_1 value by the sign of $\theta_1(t) - a$. The variation of θ_1 along the trajectory might be zero for some I_1 by Lemma 4.1.1, which means that the trajectory does not cross the initial condition of θ_1 value. In other words, θ_2 spikes but θ_1 does not spike. We call such a solution a suppressed solution. To show the existence of such a solution, we will investigate the situations that the trajectory does not cross the initial condition of θ_1 value a, which is enough to guarantee the existence of a suppressed solution.

Assume that g_c is fixed throughout this section.

Lemma 4.2.1 Let $I_1 = I_1^{top}$ such that the local maximum of the θ_1 nullcline is tangent to $\theta_2 = \pi$. There is a forward flow of $(\theta_1{}^\star, -\pi)$ that reaches (α, π) with $\theta_1{}^\star < \alpha$, where $\theta_1{}^\star$ is the local maximum point of the θ_1 nullcline.

Proof of 4.2.1

The flow on the vertical line $\theta_1 = \theta_1{}^\star$ points up and to the left. Thus the trajectory starting at $(\theta_1{}^\star, -\pi)$ does not cross the vertical line. If the trajectory hits $(\theta_1{}^\star, \pi)$, then it must approach $(\theta_1{}^\star, \pi)$ from the outside of the θ_1 nullcline due to the flow on the vertical line. So the trajectory must approach $(\theta_1{}^\star, \pi)$ tangentially because the θ_1 nullcline is tangent to $\theta_2 = \pi$. However, the vector field at $(\theta_1{}^\star, \pi)$ has only a vertical component because it is on the θ_1 nullcline. Thus it is impossible that the trajectory hits $(\theta_1{}^\star, \pi)$. Therefore, the trajectory hits the point (α, π) with $\alpha < \theta_1{}^\star$.

Now we define a function from the open interval J to the open interval M where $J = (-\pi, a)$ and $M = (-\pi, \pi)$ to describe a suppressed solution of the system (4.2) more concretely where $(a, -\pi)$ is on the backward flow of (π, π).

Definition 4.2.2 A function h_0 is defined from the interval $J = (-\pi, a)$ to $M = (-\pi, \pi)$ by the flow (4.2) $\Phi(\theta_1, \theta_2, t)$: When $\Phi(\theta_1, -\pi, t) = \Phi(\theta_1^{h_0}, \pi, 0)$ for some $\theta_1^{h_0}$ and the smallest $t > 0$, $h_0(\theta_1)$ is defined as $\theta_1^{h_0}$.

The trajectory starting at $(\theta_1, -\pi)$ hits $(\theta_1^{h_0}, \pi)$ with some $\theta_1^{h_0}$ value for the first time. Then h_0 is well-defined and continuous because of the continuity of the flow with respect to initial condition and the uniqueness of the solution. From Lemma 4.2.1, there exists θ_1 such that $h_0(\theta_1) - \theta_1 < 0$ and obviously, $h_0(-\pi) - (-\pi) > 0$. Then by intermediate value theorem, there exists θ_1^s such that $h_0(\theta_1^s) - \theta_1^s = 0$. Put $k_0(\theta_1) \equiv h_0(\theta_1) - \theta_1$. Since $k_0(-\pi) > 0, k_0(\theta_1^\star) < 0$ and $k_0(a) > 0$, there exist at least two zeros, called $\theta_1{}^{ss}, \theta_1{}^{us}$ with $\theta_1{}^{ss} < \theta_1{}^{us}$ of the function k_0 between $-\pi$ and a. The function k_0 depends on parameters I_1, g_c and I_2.
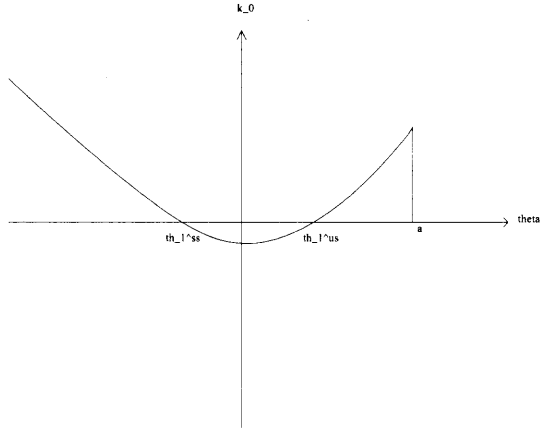
Figure 4.13 A diagram of the function k_0 shows that there exist two zeros. The diagram corresponds to the Figure 4.12, where $(a, -\pi)$ is on the backward trajectory of (π, π).

Corollary 4.2.3 Whenever $k_0(\theta_1) < 0$ for some θ_1 between $-\pi$ and a, there exist θ_1^{ss} and θ_1^{us} with $\theta_1^{ss} < \theta_1^{us}$ such that $k_0({\theta_1}^{ss}) = k_0({\theta_1}^{us}) = 0$.

Corollary 4.2.3 does not prove that there exists at most two such zeros. But it is evident that for small g_c values, the function k_0 has at most two zeros because the corresponding function k_0 of the uncoupled systems of (4.2) has at most two zeros that are both hyperbolic. Figure 4.13 shows a diagram for the function k_0 with $I_1 = I_{top}$ which makes the local maximum of θ_1 nullcline tangent to $\theta_2 = \pi$ and the only two zeros of function k_0. Therefore, the existence of zeros of function k_0 corresponds to the existence of suppressed solutions. Obviously, ${\theta_1}^{ss}$ corresponds to the stable suppressed solution and ${\theta_1}^{us}$ to the unstable one.

Corollary 4.2.4 The stable suppressed solution is globally stable in the phase space.

By resetting the θ_2 value to $-\pi$, every trajectory falls into $(-\pi, 0) \times -\pi$. Then the trajectory is attracted to the stable suppressed solution because it does not cross the suppressed solution.

From Lemma 4.2.1, note that $\frac{\partial k}{\partial I_1}$ is positive. So there is no suppressed solution for large enough $I_1 > 0$ values, which means that $k_0 > 0$ for such large I_1.

Corollary 4.2.5 The two suppressed solutions approach each other and disappear as I_1 increases through a value denoted $I_1{}^{ds}$.

Now we investigate suppressed solutions by varying conductance g_c. Given some $I_1 < 0$, the conductance g_c can be chosen small enough to let the system have a suppressed solution from Property 9 and Lemma 4.2.1.

Corollary 4.2.6 For given fixed $I_1 < 0$, there exists an interval of $g_c > 0$ values such that the coupled system (4.2) has a stable and unstable suppressed solution.

4.3 $1 : N$ Spiking Solutions

As I_1 increases, the function k_0 has no zeros and become positive. In other words, the two suppressed solutions disappear and they are replaced by $1 : N$ (the θ_1 spiking frequency to θ_2 one) spiking. Finally, as I_1 increases up to I_2, there exists the synchronous solution.

Until now we have chosen $H(\theta_1, \theta_2) = \theta_1 - \theta_2$. An issue with this choice is that at $\theta_i = \pi$, $i = 1$, 2 when we reset, it yields non-smoothness of the flow. However if we choose $H(\theta_1, \theta_2) = sin(\theta_1 - \theta_2)$, then the flow is smooth. This allows to consider Denjoy's Theorem associated with circle maps [28]. Since the nullclines and the vector fields for the case $H(\theta_1, \theta_2) = \theta_1 - \theta_2$ are similar to that of $H(\theta_1, \theta_2) = sin(\theta_1 - \theta_2)$ except near $\theta_i = \pi$, $i = 1$, 2, we might expect that the results of the Denjoy's Theorem carry over to the case $H(\theta_1, \theta_2) = \theta_1 - \theta_2$. In the following section, we show that to be the case.

The rotation number can be interpreted as the average θ_2 rotation of a given initial condition versus θ_1 rotation under the Poincare map on the $2 - D$ torus [28]. Denjoy's Theorem shows that the rotation number number is well defined and

characterizes the qualitative features of a smooth flow on the torus. We now apply Denjoy's Theorem to our model.

Denote the flow generated by (4.2) with $H(\theta_1, \theta_2) = sin(\theta_1 - \theta_2)$ and without resetting by $\Theta(\theta_1, \theta_2, t)$. For each positive integer n, define the map $\Pi_n(\theta_2)$ from $(-\infty, \infty)$ to $(-\infty, \infty)$ by $\Pi_n(\theta) = \theta_2{}^n$: When $\Theta(-\pi, \theta_2, t) = \Theta((2n-1)\pi, \theta_2{}^n, 0)$ for the smallest t > 0 and some $\theta_2{}^n$. Finally we define the rotation number as $\rho(\Pi) = \lim_{n \to \infty} \frac{\Pi_n(\theta_2)}{2n\pi}$ for the corresponding maps Π_n. Denjoy's Theorem shows that the map Π_n and the rotation number $\rho(\Pi)$ are well-defined where Π is the corresponding Poincare's map on the $2-D$ torus.

Note that the map Π_n is defined on the entire phase plane. $\Pi_n(\theta_2)$ is the θ_2 value when the trajectory starting at $(-\pi, \theta_2)$ hits the line $\theta_1 = (2n-1)\pi$ for the first time. The rotation number can be interpreted as the average of the number of θ_2 rotations of a point $\theta_2{}^0$ under the flow versus θ_1 rotation number and also characterizes the flow on 2-D torus to describe two possibilities, periodic orbits and dense orbits (see Figure 4.14).

Denjoy's Theorem The rotation number $\rho(\Pi)$ is well-defined and is independent of the initial θ_2 value. If Π is C^2 map, then

(1) ρ is rational if and only if Π has a periodic orbit with some period.

(2) ρ is irrational if and only if every orbit of Π is dense on S^1.

(3) $\rho(\Pi_{I_1})$ is a continuous function of I_1.

Note that the rotation number $\rho(\Pi)$ is dependent on the parameter I_1. From Lemma 4.2.1, $\rho(\Pi_{I_1})$ decreases as I_1 increases. Now we restrict the range of I_1 to the interval $(I_1{}^{ds}, I_2)$ for fixed g_c and I_2 where the suppressed solutions disappear at $I_1{}^{ds}$. It is evident that as $I_1 \longrightarrow I_1{}^{ds}$, $\rho(\Pi_{I_1}) \longrightarrow \infty$. From Lemma 4.3.1, as $I_1 \longrightarrow I_2$, $\rho(\Pi_{I_1}) \longrightarrow 1$. Thus the rotation number $\rho(\Pi_{I_1})$ continuously attains the values from ∞ to 1 as I_1 increases from $I_1{}^{ds}$ to I_2. Denjoy's Theorem immediately applies to the case when $H(\theta_1, \theta_2) = sin(\theta_1 - \theta_2)$ on $[-\pi, \infty] \times [-\pi, \infty]$, since the
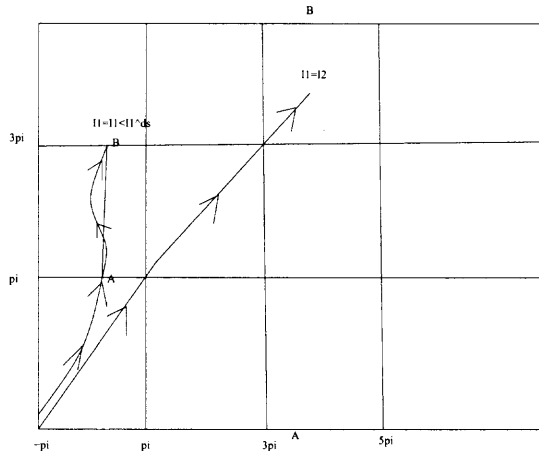
Figure 4.14 The rotation numbers $\rho(\Pi_{I_1})$ of the coupled system (4.2) has the value 1 for $I_1 = I_2$. As $I_1 \longrightarrow I_1^{ds}, \rho(\Pi_{I_1}) \longrightarrow \infty$.

vector field of (4.2) is sufficiently smooth. What we show below is that the results of the Theorem also appear to hold in the case when $H(\theta_1, \theta_2) = \theta_1 - \theta_2$.

Here we demonstrate $1 : N$ spiking, periodic $1 : N$ spiking solutions, dense orbits and other periodic solutions in the phase plane.

Lemma 4.3.1 There exists the synchronous solution when $I_1 = I_2$.

Proof of Lemma 4.3.1

Consider an initial value problem of the system (4.2) and $\theta_1(0) = -\pi, \theta_2(0) = -\pi$. Check the vector fields on the line $\theta_1 = \theta_2$.

$$\theta_1' = 1 - cos\theta_1 + I_1(1 + cos\theta_1) - g_c(\theta_1 - \theta_2) \quad = \quad 1 - cos\theta_1 + I_1(1 + cos\theta_1)$$
$$\theta_2' = 1 - cos\theta_2 + I_2(1 + cos\theta_2) - g_c(\theta_2 - \theta_1) \quad = \quad 1 - cos\theta_1 + I_1(1 + cos\theta_1)$$

Hence, $\theta_1' = \theta_2'$ on the line $\theta_1 = \theta_2$. Since the initial conditions of θ_1 and θ_2 are also on the line, the $\theta_1 = \theta_2$ is a solution of the system (4.2). Note that all trajectories starting at the line $\theta_1 = -\pi$ make $1 : 1$ spiking and return to it by resetting. Thus all trajectories make $1 : 1$ spiking.
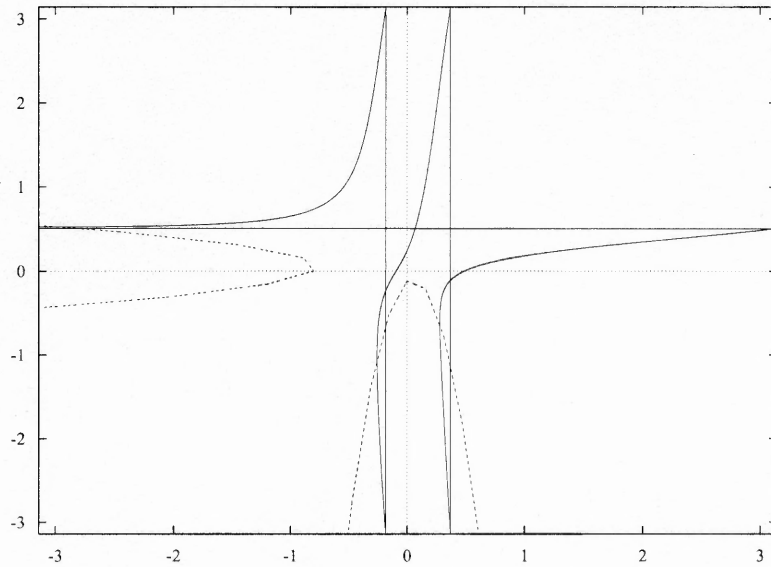
Figure 4.15 This shows 1 : 2 spiking solution where $I_1 = 0.003, I_2 = 0.02, g_c = 0.05$.

Definition 4.3.2 The system (4.2) is said to have 1 : N spiking during a finite time interval if it makes N consecutive θ_2 spikes followed by one θ_1 spike for the time window, where N is a positive integer (see Figure 4.15).

Note that 1 : N spiking does not necessarily imply a periodic solution. We now construct a 1 : 2 spike solution. Such solutions, given by Denjoy's Theorem, may actually correspond to dense orbits in the $\theta_1 - \theta_2$ phase space.

Note that the system (4.2) cannot have two consecutive θ_1 spikes as shown in Figure 4.16 in the cases for $I_1 < I_2$. Once θ_1 spikes, it resets to $\theta_1 = -\pi$. Since the forward flow of $(-\pi, -\pi)$ hits the point (α, π) where $\alpha < \pi$ by Lemma 4.2.1, Lemma 4.3.1 and $I_1 < I_2$. Thus the trajectory can not pass through the forward flow because of the uniqueness of the solution. Thus there can not be two consecutive θ_1 spikes.

Definition 4.3.3 A function h_1 is defined from the interval R to the interval S where $R = (-\pi, A)$ and $S = (B, \pi)$ shown in Figure 4.16 by the flow (4.2) $\Phi(\theta_1, \theta_2, t)$:

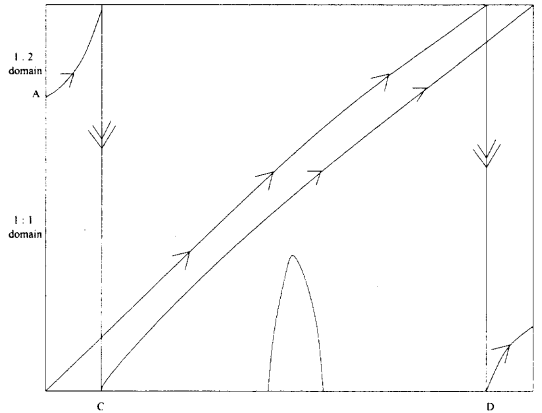**Figure 4.16** For $I_1^{dp} < I_1 < I_2$, a function h_1 is defined from $(-\pi, A)$ to (B, π). Note that the trajectories starting on $-\pi \times (A, \pi)$ have $1 : 2$ spiking before their first returns to $\theta_1 = -\pi$ and the trajectories starting on $-\pi \times (-\pi, A)$ have $1 : 1$ spiking before their first returns to $\theta_1 = -\pi$. Note that the backward flow of (π, π) hits C and the forward flow of $(-\pi, -\pi)$ reset to $(D, -\pi)$.

When $\Phi(-\pi, \theta_2, t) = \Phi(\pi, \theta_2^{h_1}, 0)$ for some $\theta_2^{h_1}$ and the smallest t >0, $h_1(\theta_2)$ is defined as $\theta_2^{h_1}$.

Denote the function $k_1(\theta_2)$ by $h_1(\theta_2) - \theta_2$. Note also that a function $h_2(\theta_2)$ can be defined similarly from the interval (A, π) to the interval $(-\pi, B)$ to capture $1 : 2$ spiking. As shown in Figure 4.16, for a small perturbed value I_1 from I_2, $I_2 - I_1 < \epsilon$, a trajectory moves up and more to the left. Thus the forward flow of $(-\pi, -\pi)$ hits (D, π) where $D < \pi$ and the backward flow hits $(-\pi, C)$ where $C > -\pi$. The effects of I_1 on the flow are systematically summarized in Remark 4.3.4. The trajectories starting on $-\pi \times (A, \pi)$, called $1 : 2$ domain, yield a transient $1 : 2$ spiking and reset to enter the domain of $1 : 1$ spiking. Thus in this set of parameters, a transient $1 : 1$ and $1 : 2$ spiking co-exists. We describe the dynamics with the k_1 and k_2 functions. Here it is evident that $k_1(A^-) > 0$ and $k_1(-\pi^+) > 0$ due to the continuity of flow with respect to initial conditions. But the sign of $k_1(\theta_2)$ between A and $-\pi$ is not clear. Denjoy's Theorem guarantees the existence of a $1 : 1$ periodic solution. If $k_1(\theta_2) < 0$ for some $-\pi < \theta_2 < A$ and thus there exists a zero of k_1 by the intermediate value
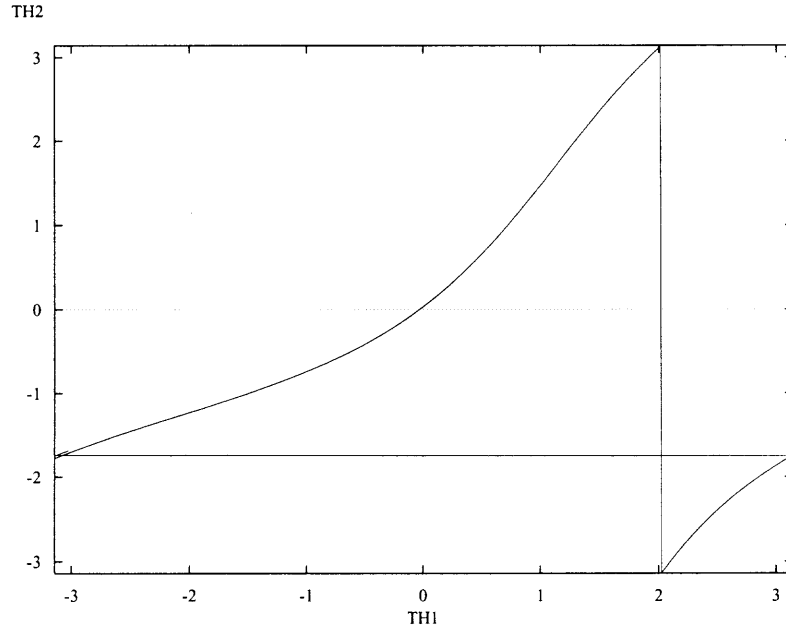
Figure 4.17 For $I_1{}^{dp} < I_1 < I_2$, the trajectory starting at approximately $(-\pi, -1.78)$ makes $1:1$ spiking and returns to its starting point, which allows a $1:1$ periodic solution and it is simulated by XPP, where $I_1 = 0.0175, I_2 = 0.02, g_c = 0.05$.

theorem. Hence there exists a $1:1$ periodic spiking solution for $I_1{}^{dp} < I_1 < I_2$ where $I_1{}^{dp}$ is indicated in Remark 4.3.4 (see Figure 4.17). $k_2 < 0$ for (A, π), which means that a trajectory starting at $1:2$ domain must leave this region by resetting and is attracted to the periodic $1:1$ spiking solution. A numerical simulation supports the existence of this periodic solution as shown in Figure 4.17.

Remark 4.3.4 As in Figure 4.18, $\lim_{I_1 \to I_2^-} A = \pi$, $\lim_{I_1 \to I_2^-} B = -\pi$, $\lim_{I_1 \to I_2^-} C = -\pi$, $\lim_{I_1 \to I_2^-} D = \pi$ and $\lim_{I_1 \to I_1^{12}} C = \lim_{I_1 \to I_1^{12}} D$, $\lim_{I_1 \to I_1^{12}} A = -\pi$, $\lim_{I_1 \to I_1^{12}} B = \pi$, where I_1^{12} is the I_1 value for which the forward flow of $(-\pi, -\pi)$ coincides with the backward flow of (π, π) as in Figure 4.23.

As $I_1 \to I_2^-$, $A(B)$ moves up to $\pi(-\pi)$. As I_1 decreases, $A(B)$ moves up to $-\pi(\pi)$. For some I_1 value, C and D coincide. We call the I_1 value $I_1{}^{dp}$. Note that $I_1{}^{12} < I_1{}^{dp} < I_2$

Remark 4.3.5 There exists an $I_1{}^{dp}$ such that $A = B$ for $I_1{}^{12} < I_1{}^{dp} < I_2$.
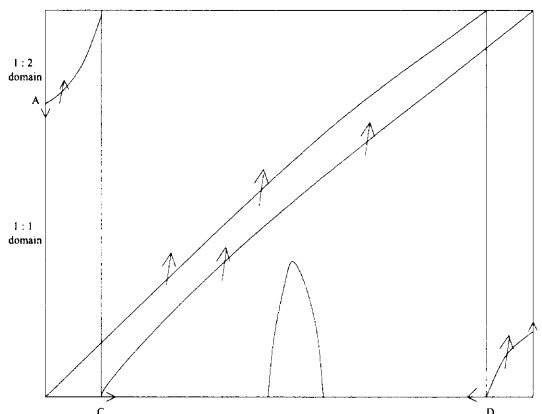
Figure 4.18 This shows the vector fields for a smaller I_1 value than Figure 4.16 on some curves that are trajectories for I_1 value of Figure 4.16. The flows on those curves point up and to the left. Thus A and D decrease but B and C increase as I_1 decreases. By the same argument, as I_1 increases, A and D increase but B and C decrease.
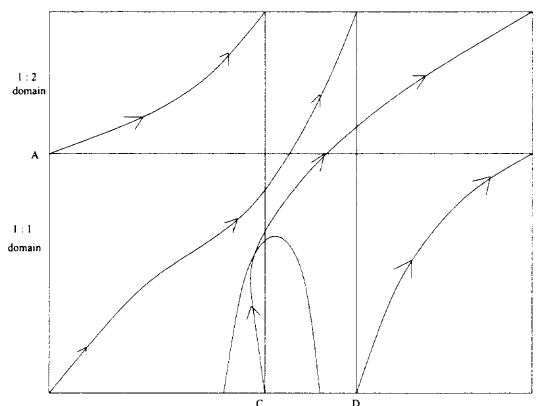
Figure 4.19 For $I_1 = I_1{}^{dp}$, the trajectory starting at $(-\pi, A)$ hits (C, π), resets to $(C, -\pi)$, hits (π, π), resets to $(-\pi, -\pi)$, hits (D, π), resets to $(D, -\pi)$, hits (π, B) and resets to its starting position $(-\pi, A)$. The cycle repeats.
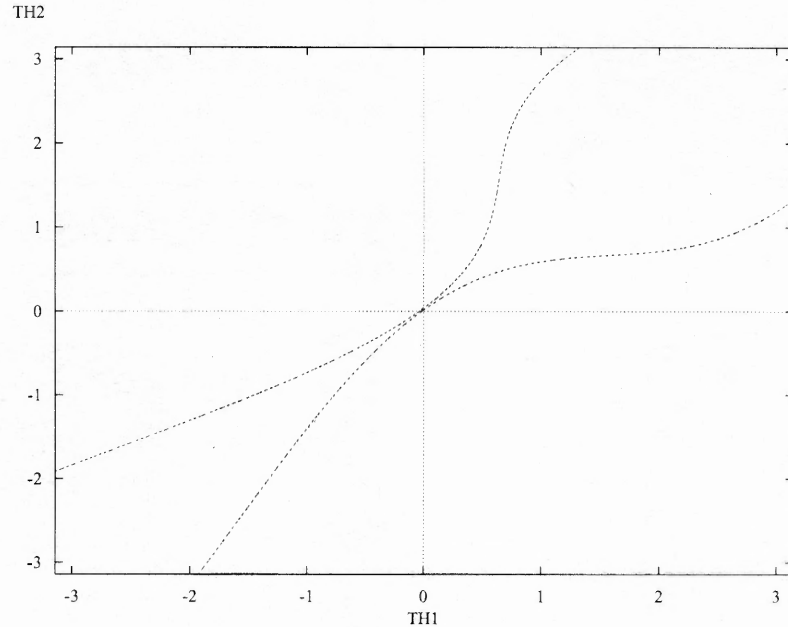
Figure 4.20 When $I_1 = I_1{}^{dp}$, the union of orbits of k_1 and k_2 at a certain point of either domain is dense in $[-\pi, \pi]$ where $I_1 = I_1{}^{dp} = 0.005, I_2 = 0.02, g_c = 0.05$.

When $I_1 = I_1{}^{dp}$, the system (4.2) yields a periodic solution as shown in Figure 4.19. In this set of parameters, there exists a periodic solution as shown in Figure 4.19 which is different from $1 : N$ solution. But $k_1 > 0$ and thus every trajectory starting in the $1 : 1$ domain can not stay in and enters the $1 : 2$ domain. $k_2 < 0$ and also every trajectory on the $1 : 2$ domain must enter the $1 : 1$ domain. If we consider a trajectory that starts at a certain point in the domain $1 : 1$ and first returns to a point in the $1 : 1$ domain, it is not clear if its return point is exactly the starting point. If its return point is the starting point, there exists another periodic solution which is not $1 : N$ type but of mixed type where θ_2 first spikes, then θ_1 and θ_2 spike simultaneously, then θ_2 spikes, then θ_1 spikes and the process corresponds to a repetition. As long as there are no such points for any next cycles, the union of orbits of k_1 and k_2 at a point of either domain must correspond to a dense orbit in $[-\pi, \pi]$ as shown in Figure 4.20.
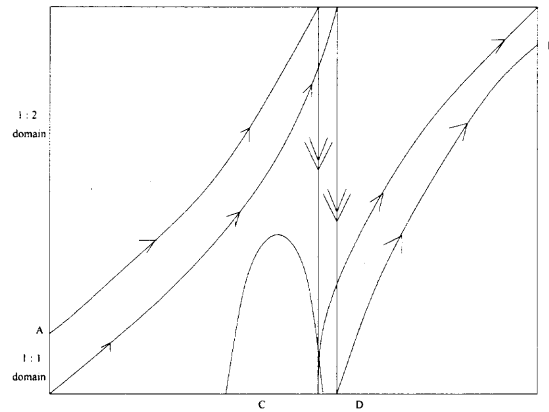
Figure 4.21 When $I_1{}^{12} < I_1 < I_1{}^{dp}$, then $k_1 > 0$ and thus every trajectory starting on the 1 : 1 domain enters the 1 : 2 domain. But $k_2(A^+) < 0$ and $k_2(\pi^-) < 0$. So there might be some possibility for the system (4.2) to have a stable 1 : 2 periodic solution if there is $k_2(\theta_2) > 0$ for some θ_2.
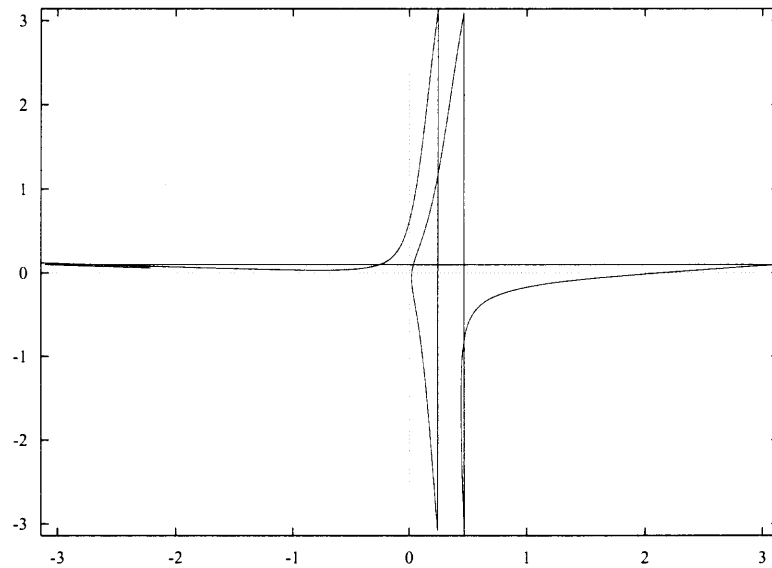
Figure 4.22 When $I_1{}^{12} < I_1 < I_1{}^{dp}$, a numerical simulation by XPP shows the existence of a 1 : 2 periodic solution, where $I_1 = 0.002, I_2 = 0.02, g_c = 0.05$.
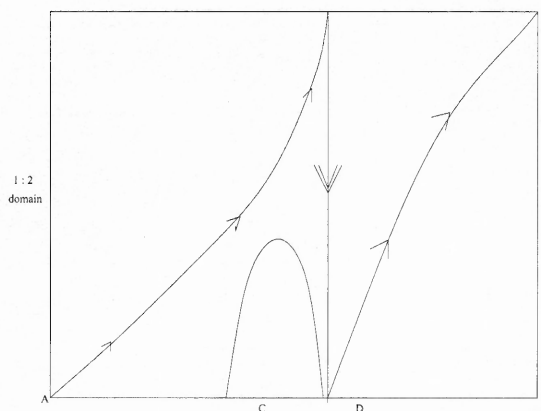
Figure 4.23 For $I_1 = I_1{}^{12}$, the forward trajectory of $(-\pi, -\pi)$ and the backward trajectory of (π, π) coincide. So only $1 : 2$ spiking appears.
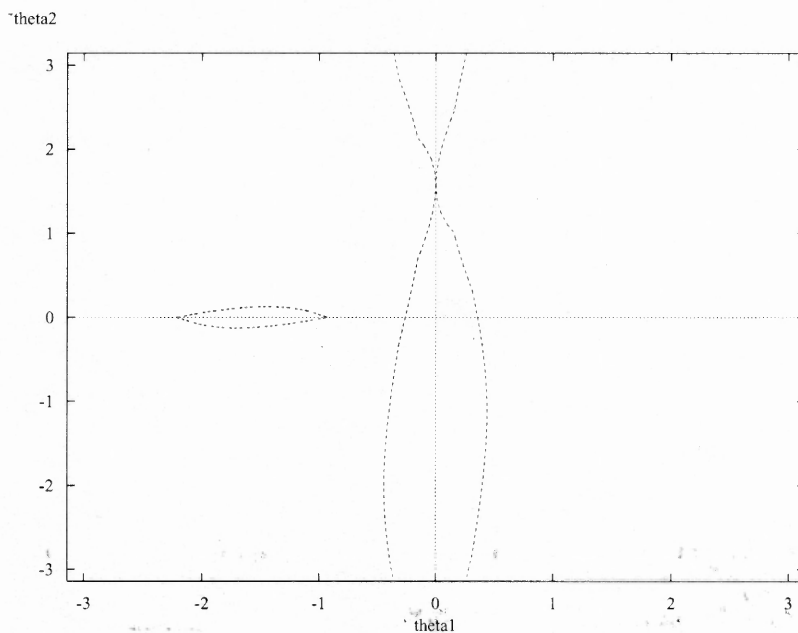
Figure 4.24 In the case $H(\theta_1, \theta_2) = sin(\theta_1 - \theta_2)$, the θ_1 nullcline enclosing the θ_2 axis separates the whole phase plane into the two sections. The θ_2 nullcline is the closed curve that surrounds some part of θ_1 axis where $g_c = 0.05$, $I_1 = -0.015$, $I_2 = 0.02$.

Since the rotation number $\rho(\Pi)$ takes the values $(1, \infty)$, there exists a $1 : N$ periodic solution for any positive integer N. Figure 4.21 can be similarly explained as in Figure 4.16. As I_1 decreases to $I_1{}^{12}$, only $1 : 2$ spiking appears. Furthermore, we can explain $1 : 3$ and even $1 : N$ spiking for $N \geq 4$ in a similar manner.

Now we see how the vector fields and nullclines of the two different functions $H(\theta_1, \theta_2) = \theta_1 - \theta_2$ and $H(\theta_1, \theta_2) = sin(\theta_1 - \theta_2)$ are compared.

1. Since $\frac{\partial F}{\partial I_1}$ are the same for the two different functions $H(\theta_1, \theta_2) = \theta_1 - \theta_2$ and $H(\theta_1, \theta_2) = sin(\theta_1 - \theta_2)$, all flow properties that depend on I_1 are the same for either case $H(\theta_1, \theta_2)$. Since we have fixed I_2 and g_c in this section, we expect that the dynamics of the flow of the two different $H(\theta_1, \theta_2)$ are quite similar.

2. As shown in Figure 4.24, the θ_1 nullcline separates phase plane into the two sections where a trajectory starting on the left side of the left branch of the θ_1 do not cross the branch. Thus there exits θ_1 such that $k_0(\theta_1) < 0$, which allows a suppressed solution. Decreasing I_1 clearly makes the function k_0 more negative as like the case of $H(\theta_1, \theta_2) = \theta_1 - \theta_2$.

4.4 Conclusion

The results of this chapter demonstrate that even a simple model of two gap-junctionally coupled theta neurons can exhibit surprisingly complicated behavior. This should be contrasted with the case of two synaptically coupled theta neurons in which the typical behaviors are much narrower. Two synaptically coupled model theta neurons drive the system to be synchronous. Thus the gap-junctional coupling plays a role of expanding the dynamic capability of this network. Our geometric construction of solutions allows us to understand the stability of certain solutions that were obtained from Denjoy's theorem. As shown in Figure 4.1 and 4.2 for large values of g_c, the trajectories in a region of the first quadrant between the two nullclines tend to be

synchronous. So as g_c increases, the two nullclines approach the line $\theta_1 = \theta_2$ and thus the trajectories between them tend to be more synchronous.

As Figure 4.17, even after the suppressed solutions disappear, the trajectories are attracted to some region on the left side of the θ_1 nullcline and then are expanded on the right side of the θ_1 nullcline. It still remains an open question to measure whether the function h_n is contracted. We will use Lemma 4.1.2 and Lemma 4.1.3 in pursuit of the contraction.

CHAPTER 5

CONCLUSION

5.1 Summary and Discussion

There is much evidence showing the presence of gap junctions in neuronal networks. The roles of gap junctions in neuronal networks have begun to be understood. At electrical synapses (gap junctions), current flows directly into the post synaptic cell. Thus transmission across electrical synapses is very fast.

Gansert, Nadim and Golowasch studied sustained activity in a random network coupled by gap junctions [19]. By detecting the kernel of network activity, they found that activity can be sustained within this sub-network. They specifically studied how activity depends on cable diameter and showed that activity can be sustained through network in a neighborhood of the optimal diameter. The first part of this thesis was motivated by this work of Gansert, Nadim and Golowasch.

We first considered a deterministic neuronal network of identical point cells. We wanted to know whether activity propagates through and is sustained by the network. Specifically, we investigated how sustainment of activity depends on network connectivity, the refractory period of each neuron and the number of associated paths. A necessary condition for sustainment of activity is the existence of a sup cut-off node. Whether activity is sustained can be deduced by knowing whether activity propagates through a cut-off node. Nodes having different initial refractory states within a neighborhood of the stimulated node influence network activity. We have found that whether an action potential propagates through a cut-off node with n connections at a discrete time t ends up with knowing whether $\frac{P(a,i,t)-R(a,i,b,t)}{n-P(a,i,t)+R(a,i,b,t)}$ is greater than the threshold. The numerator indicates the number of all paths having length t other than the paths including node b that is in a neighborhood of the

initiated node a and has a different refractory state. Thus the effective current flux at a given time t is $\frac{P(a,i,t)-R(a,i,b,t)}{n-P(a,i,t)+R(a,i,b,t)}$. An increased refractory period has the effect of reducing the network activity passing through a given cell (see example 2.2.2). However, reducing activity propagation at a certain node does not mean that the possibility of sustaining network activity decreases (see example 2.2.2). An increased degree of a node also reduces network activity propagation because a node needs more in-flowing currents at a given time. We showed that network activity dies off because the current flux at a given node was too small or because the cell was in a refractory state when the activity arrived. the propagation time for the two coupled cables will not be a unit time but can be expressed in terms of diameter and the strength of coupling resistance. When we replace point cells in network architectures found in Chapter 2 with spatially dependent neurons, activity might be sustained or die off by adjusting diameter because it controls the voltage response and the activity propagation time related to the refractory state.

Nadim and Golowasch have shown that an optimal signal transmission between two gap junctionally passive cables occurs at a specific cable diameter [20]. We have built a mathematical model for gap junctionally coupled cables in response to general inputs. The model has a discontinuity at the gap junction location, which yields a discontinuous P.D.E. We derived a linear integral equation which is equivalent to the model. This integral equation has an advantage in that it can be solved for any type of inputs.

In particular, we have derived an analytic form of the stationary solution in response to periodic waves. From the solution, we have shown that there exists an optimal diameter for which the maximum voltage amplitude of the second cable is obtained. As in an isopotential cell, the voltage response decreases as the input frequency ω increases because this attenuation is due to the distributed membrane capacitance that soaks up more and more of the current as the frequency increases

[24]. We have observed that there exists an optimal for which the phase shift can be minimized for a certain range of input frequencies by plotting the solution. We have found a sufficient condition for the existence of an optimal diameter of the voltage response in any network architecture. The sufficient condition requires that the absolute value of the voltage flux at the proximal end is bounded by $\frac{K}{d^\alpha}$ $\alpha >$ 1, $K > 0$. In other words, the boundary contribution to the solution must vanish as d increases to ∞. A current clamp exactly fits this case. But the voltage response at the proximal end is fixed for any diameter in the case of voltage clamp. Thus there is still a boundary contribution to the solution even for large values of diameter. For gap junctionally coupled cables, the voltage response resembles the case of a current clamp because the voltage flux at the proximal end is bounded by $\frac{K}{d^\alpha}$. Hence there exists an optimal diameter for the voltage response.

Finally we studied the dynamics of two theta neurons coupled by gap junctions. Depending on an intrinsic parameter I of the theta neuron and on the coupling strength g_c, the network exhibits several types of solutions including stable suppressed, $1 : N$ and $1 : 1$ spiking solutions. Here a suppressed solution and $1 : N$ spiking solution are the solutions that have the ratio of two cells' spiking frequencies as 0 and $\frac{1}{N}$, respectively. We used phase plane analysis to demonstrate the existence of the solutions. We observed that two such neurons coupled by a gap junction also yield a saddle node bifurcation in the sense that the ratio of two cells' spiking frequencies changes with coupling strength g_c and their model intrinsic parameter I from a very low frequency for a large positive integer N . In other words, there is a transition between a suppressed solution and $1 : N$ spiking solution. This is analogous to the signal transmission of coupled cells done by Lewis and Keener [29]. Furthermore, the ratio $\frac{1}{N}$ increases up to 1 as I or g_c increases, which is consistent with Denjoy's circle map theorem [28].
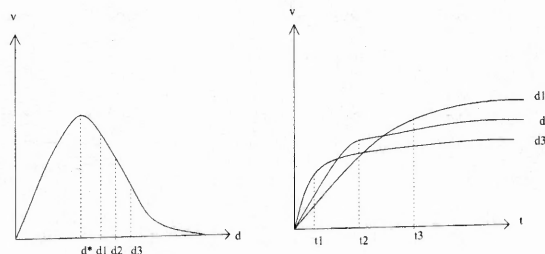
Figure 5.1 The voltage response $v_2(x, t, d)$ rises up fast for small times with large diameter values $d_1, d_2 > d^\star$.

5.2 Future Work

Regarding the first project, we will investigate how activity can propagate from a sup cut-off to the stimulated node for a more general network architecture. In the case where these are either no or more than one sup cut-off nodes, we will study how sustainment of activity can be achieved.

We are interested in combining the graph theoretic gap junctionally coupled network (each cell is isopotential) and the voltage response properties of the two gap junctionally coupled cables (each cell is non-isopotential) to understand how activity is sustained through gap junctionally coupled networks. So we will generalize our model to consider spatially dependent neurons to understand the role of cable diameter in sustained activity.

Regarding the second project, we will consider a neuron consisting of a passive dendrite coupled to an active axon. We will then couple two such neurons by gap junctions along their dendrites. If the voltage response invoked by an action potential is above a threshold, then the activity is able to propagate through the neuron. Using the abstract networks that sustain activity found from our graph theoretic work, we plan to replace the point cells by these spatially dependent active neurons to determine how sustainment of activity depends on cable diameter. We hope to prove the conjecture that by choosing the proper range of diameters, a relevant signal can be transmitted most effectively.
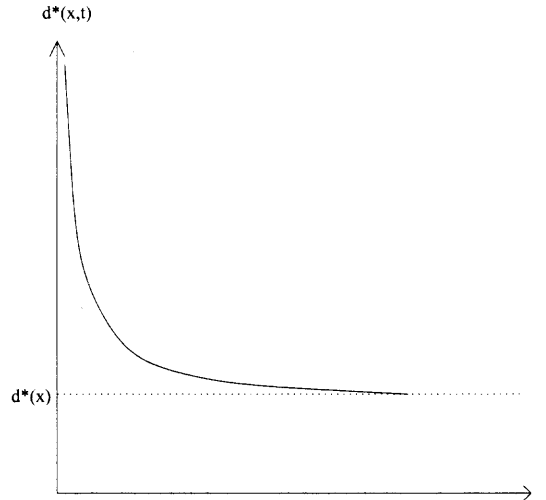
Figure 5.2 A optimal diameter $d^\star(x,t)$ decreases and approaches the optimal diameter of the steady state voltage response as $t \longrightarrow \infty$.

As seen in Theorem 3.6.8, the optimal diameter $d^\star(x,t)$ is dependent on t for fixed x. For the case of a step voltage clamp, from Conclusion of Chapter 3, we expect that the voltage response rises up fast for a large diameter value (see Figure 5.1). Thus for a small time t, $d(x,t)$ would be large. Hence we conjecture Figure 5.2 and hope to prove it mathematically. From the optimal diameter of the steady state solution, a given threshold, there exists an interval $[d_1, d_2]$ of diameters for which the voltage responses for $d \leq d_1$ or $d \geq d_2$ values can not reach the threshold (see Figure 5.3). Thus the propagation times for $d = d_1$ and d_2 would be ∞. Therefore there exists an diameter d of the shortest propagation time where the voltage response reaches the threshold first (see Figure 5.3). From conjecture of Figure 5.1, d would be greater than $d^\star$. It again remains an open question to prove it mathematically.

We are also interested in understanding the dynamics and effects of back propagation of action potentials from soma-to-dendrite. Specifically, we are interested in sustained activity where two compartments of an excitable cell burst in anti-phase and then have refractory states simultaneously. This has been referred to as ping-pong [30]. Reflected waves (back propagation) has previously been observed in an inhomogeneous
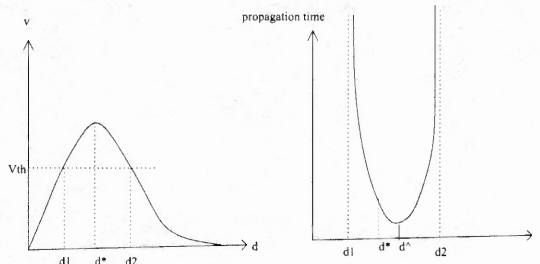
Figure 5.3 This shows the existence of an optimal diameter d for the shortest propagation time where the voltage response reaches the threshold first. Note that $d > d^\star$.

excitable cable [31]. This model exhibits wave-transmissions, reflected waves and block-transmissions as diameter changes abruptly with distance. Cable diameter plays a role in whether or not back propagation of action potentials occurs. Inhomogeneity acts like a gap junction. As the diameter of cable 2 increases, the voltage flux at the proximal end of cable 2 decreases to zero and hence wave-block occurs. However, there are no optimal diameters for the best signal effectiveness because the cables are excitable. We want to build a two compartment model that is able to allow two compartments to have back propagation and refractory states simultaneously.

Regarding the third project, we also observed that there appears to be a stable river which is a trajectory that attracts all other trajectories in a certain region in phase space. The stable river is a stable suppressed or $1 : N$ solution and depends on I and g_c. It globally attracts all trajectories in phase plane and thus allows a stable suppressed or $1 : N$ solution to be globally stable. A stable river has previously been observed in a single theta neuron model by Borgers and Kopell [27]. It remains an open question why rivers exist in the theta neuron model and is part of the future work which we will pursue.

BIBLIOGRAPHY

[1] B. Connors and M. Long, "Electrical synapses in the mammalian brain," *Annual Review of Neuroscience*, vol. 27, pp. 393–418, 2004.

[2] T. Lewis and J. Rinzel, "Dynamics of spiking neurons connected by both inhibitory and electrical coupling," *Journal of Computational Neuroscience*, vol. 14, pp. 283–309, 2003.

[3] B. Ermentrout, "Gap junctions destroy persistent states in excitatory networks," *Physica Review E*, vol. 74, p. 0311918(8), 2006.

[4] C. Chow and N. Kopell, "Dynamics of spiking neurons with electrical coupling," *Neural Computation*, vol. 12, pp. 1643–1678, 2000.

[5] T. Lewis, "Phase-locking in electrically coupled non-leaky integrate-and-fire neurons," *Discrete and Continuous Dynamical Systems-Series B*, vol. Supplement, pp. 554–562, 2003.

[6] F. Hoppensteadt and E. Izhikevich, *Weakly Connected Neural Networks*. New York: Springer-Verlag, third ed., 1997.

[7] B. Ermentrout, "Synchronization in a pool of mutually coupled phase oscillators with random frequencies," *Journal of Mathematical Biology*, vol. 22, pp. 1–9, 1985.

[8] B. Ermentrout and N. Kopell, "Symmetry and phase locking in chains of weakly coupled oscillators," *Comm. Pure Appl. Math*, vol. 49, pp. 623–660, 1986.

[9] B. Ermentrout and N. Kopell, "Phase transitions and other phenomena in chains of coupled oscillators," *Siam J. Appl. Math.*, vol. 50, pp. 1014–1052, 1990.

[10] L. Ren and B. Ermentrout, "Monotonicity of phase locked solutions in chains and arrays of nearest-neighbor coupled oscillators," *Siam J. Math. Anal.*, vol. 29, pp. 208–234, 1998.

[11] L. Ren and B. Ermentrout, "Phase-locking in chains of multiple-coupled oscillators," *Physica D*, vol. 143, pp. 56–73, 2000.

[12] S. Strogatz, "From kuramoto to crawford: Exploring the onset of synchronization in populations of coupled oscillators," *Physica D*, vol. 143, pp. 1–20, 2000.

[13] G. Medvedev and N. Kopell, "Synchronization and transient dynamics in the chains of electrically coupled fitzhugh nagumo oscillators," *Siam J.Appl. Math.*, vol. 61, pp. 1762–1801, 2001.

[14] C. Wilson and J. Callaway, "Coupled oscillator model of the dopaminergic neuron of the substantia nigra," *Journal of Physiology*, vol. 83, pp. 3084–3100, 2000.

[15] W. Gerstner and W. Kistler, *Spiking Neuron Models*. London: Cambridge University Press, first ed., 2002.

[16] R. Eisenberg and E. Johnson, "Three-dimensional electrical field problems in physiology," *Prog. Biophys. Mol. Biol.*, vol. 20, pp. 1–65, 1970.

[17] W. Rall, "Core conductor theory and cable properties of neurons in handbook of physiology, the nervous system and cellular biology of neurons.," *AM. Physiol. Soc*, vol. 1, pp. 39–97, 1977.

[18] H. Tuckwell, *Introduction to Theoretical Neurobiology: Volume 1*. London: Cambridge University Press, second ed., 1988.

[19] J. Gansert, J. Golowasch, and F. Nadim, "Gap-junctionally coupled networks of model neurons depends on the diameter of coupled dendrites," *Journal of Neurophysiology*, vol. 98, pp. 3450–3460, 2007.

[20] F. Nadim and J. Golowasch, "Signal transmission between gap junctionally coupled passive cables is most effective at an optimal diameter," *Journal of Neurophysiology*, vol. 95, pp. 3831–3843, 2006.

[21] B. Ermentrout and N. Kopell, "Parabolic bursting in an excitable system coupled with a slow oscillation," *SIAM J. Appl. Math.*, vol. 46, pp. 233–253, 1986.

[22] N. Deo, *Graph Theory with Applications to Engineering and Computer Science*. New Jersey: Prentice-Hall, 2nd ed., 1974.

[23] R. Martin, J. Nicholas, B. Wallace, and P. Fuchs, *From Neuron to Brain*. Sunderland, MA: Sinauer Associates Inc, fourth ed., 2001.

[24] C. Koch, *Biophysics of Computation*. New York: Oxford University Press, first ed., 1999.

[25] L. Evans, *Partial Differential Equations*. Rhode Island: AMS, first ed., 1998.

[26] W. Holmes, "The role of dendritic diameters in maximizing the effectiveness of synaptic inputs," *Brain Research*, vol. 478, pp. 127–137, 1989.

[27] C. Borgers and N. Kopell, "Effects of noise on rhythms in networks of excitatory and inhibitory neurons," *Neural Computation*, vol. 17, pp. 557–608, 2005.

[28] J. Hale and H. Kocak, *Dynamics and Bifurcations*. New York: Springer-Verlag, first ed., 1991.

[29] T. Lewis and J. Keener, "Wave-block in excitable media due to regions of depressed excitability.," *Siam J.Appl. Math.*, vol. 61, pp. 293–316, 2000.

[30] X.-J. Wang, "Fast burst and short-term synaptic plasticity: A model of neocortical chattering neurons," *Neuroscience*, vol. 89, pp. 347–362, 1999.

[31] B. Ermentrout and J. Rinzel, "Reflected waves in an inhomogeneous excitable medium," *Siam J. Appl. Math.*, vol. 56, pp. 1107–1128, 1996.